Commun. Comput. Phys.
doi: 10.4208/cicp.300410.300710a

Vol. **10**, No. 2, pp. 474-508
August 2011

Local Discontinuous Galerkin Methods for the Degasperis-Procesi Equation

Yan Xu[1,*] and Chi-Wang Shu[2]

[1] *Department of Mathematics, University of Science and Technology of China, Hefei 230026, Anhui, China.*
[2] *Division of Applied Mathematics, Brown University, Providence, RI 02912, USA.*

Received 30 April 2010; Accepted (in revised version) 30 July 2010

Available online 28 April 2011

Abstract. In this paper, we develop, analyze and test local discontinuous Galerkin (LDG) methods for solving the Degasperis-Procesi equation which contains nonlinear high order derivatives, and possibly discontinuous or sharp transition solutions. The LDG method has the flexibility for arbitrary h and p adaptivity. We prove the L^2 stability for general solutions. The proof of the total variation stability of the schemes for the piecewise constant P^0 case is also given. The numerical simulation results for different types of solutions of the nonlinear Degasperis-Procesi equation are provided to illustrate the accuracy and capability of the LDG method.

AMS subject classifications: 65M60, 35Q53

Key words: Local discontinuous Galerkin method, Degasperis-Procesi equation, L^2 stability, total variation stability.

1 Introduction

In this paper, we consider numerical approximations to the Degasperis-Procesi (DP) equation

$$u_t - u_{txx} + 4f(u)_x = f(u)_{xxx}, \tag{1.1}$$

where $f(u) = u^2/2$. We develop two local discontinuous Galerkin (LDG) methods for this nonlinear DP equation. Our proposed schemes are high order accurate, nonlinear stable and flexible for arbitrary h and p adaptivity. The proof of the L^2 stability of the schemes are given for general solutions and total variation stability for the piecewise constant P^0 case is also given. To our best knowledge, this is the first provably stable finite element method for the DP equation.

*Corresponding author. *Email addresses:* yxu@ustc.edu.cn (Y. Xu), shu@dam.brown.edu (C.-W. Shu)

Degasperis and Procesi [14] studied the following family of third order dispersive PDE conservation laws,

$$u_t+c_0u_x+\kappa u_{xxx}-\epsilon^2u_{txx}=(c_1u^2+c_2u_x^2+c_3uu_{xx})_x, \tag{1.2}$$

where κ, ϵ, c_0, c_1, c_2, and c_3 are real constants. Their motivation was to answer the question of which equations of a form similar to the Camassa-Holm (CH) equation are integrable. Applying the method of asymptotic integrability to the family (1.2), they found that there are only three equations that satisfy the asymptotic integrability condition within this family, namely, the KdV equation ($\epsilon=c_2=c_3=0$), the CH equation ($c_1=-3c_3/2\epsilon^2$, $c_2=c_3/2$) and one new equation ($c_1=-2c_3/2\epsilon^2$, $c_2=c_3$, the DP equation). By rescaling, shifting the dependent variable and applying a Galilean boost [13], one can find the Degasperis-Procesi equation (1.1) which has a similar form to the limiting case of the Camassa-Holm shallow water equation.

Despite the similarities to the CH equation, we would like to point out that the DP equation is truly different. One of the important features of the DP equation is that it has not only peaked solutions [13], for example, $u(x,t)=ce^{-|x-ct|}$, but also shock waves to the equation [9,24], for example

$$u(x,t)=-\frac{1}{t+c}\text{sign}(x)e^{-|x|}, \quad c>0. \tag{1.3}$$

Also, these two equations have entirely different forms of conservation laws:

- Three useful conservation laws for the DP equation:

$$E_1(u)=\int_R(u-u_{xx})dx, \quad E_2(u)=\int_R(u-u_{xx})vdx, \quad E_3(u)=\int_R u^3dx,$$

  where $4v-v_{xx}=u$.

- Three useful conservation laws for the CH equation:

$$H_1(u)=\int_R(u-u_{xx})dx, \quad H_2(u)=\int_R(u^2+u_x^2)dx, \quad H_3(u)=\int_R(u^3+uu_x^2)dx.$$

We can see that the corresponding conservation laws of the DP equation are much weaker than those of the CH equation. The conservation laws $E_i(u)$ can not guarantee the boundedness of the slope of a wave in the L^2-norm. There is no way to find conservation laws controlling the H^1-norm, which plays a very important role in studying the CH equation. Such nonlinearly dispersive partial differential equations support peakon solutions and shock solutions. The lack of smoothness of the solution introduces more difficulty in the numerical computation. It is a challenge to design stable and high order accurate numerical schemes for solving this equation.

In the last ten years, a lot of analysis has been given for the DP equation. Coclite and Karlsen proved existence and uniqueness results for entropy weak solutions belonging to the class $L^1\cap BV$ in [9] and uniqueness result for entropy weak solutions by replacing the Kruzžkov-type entropy inequalities by an Oleinik-type estimate in [10]. For

the wellposedness of the initial value problem, Yin has given a discussion within certain functional classes in a series of papers [39–41]. Some blowup results were studied in [16,17,23].

The explicit form of multipeakon solutions of the DP equation was found by Lundmark and Szmigielski [25,26]. Lundmark [24] found some explicit shock solutions to the DP equation that are entropy weak solutions and also showed that a jump discontinuity forms when a peakon collides with an antipeakon. The traveling wave solutions of the DP equation were investigated in [21]. Matsuno [27,28] discussed multisoliton solutions and their peakon limits and N soliton solutions of the DP equation.

There are only a few numerical works in the literature to solve the DP equation. Coclite, Karlsen and Risebro [11] constructed several operator splitting schemes and proved that solutions of these finite difference schemes converge to entropy weak solutions. Moreover, they provided several numerical examples to show that shock solutions can form independently of the smoothness of the initial data. Another operator splitting method was proposed for the DP equation in [18], which is based on the second-order TVD scheme and linearized implicit finite difference method. In [20], a particle method based on the multi-shock peakon solutions was investigated for entropy weak solutions of the DP equation numerically.

The discontinuous Galerkin (DG) method we discuss in this paper is a class of finite element methods, using discontinuous, piecewise polynomials as the solution and the test space. It was first designed as a method for solving hyperbolic conservation laws containing only first order spatial derivatives, e.g., Reed and Hill [29] for solving linear equations, and Cockburn et al. [2–4, 6] for solving nonlinear equations. It is difficult to apply the DG method directly to the equations with higher order derivatives. The LDG method is an extension of the DG method aimed at solving partial differential equations (PDEs) containing higher than first order spatial derivatives. The first LDG method was constructed by Cockburn and Shu in [5] for solving nonlinear convection diffusion equations containing second order spatial derivatives. Their work was motivated by the successful numerical experiments of Bassi and Rebay [1] for the compressible Navier-Stokes equations. The idea of the LDG method is to rewrite the equations with higher order derivatives into a first order system, then apply the DG method on the system. The design of the numerical fluxes is the key ingredient to ensure stability. The LDG techniques have been developed for convection diffusion equations (containing second derivatives) [5], nonlinear one-dimensional and two-dimensional KdV type equations [33,38] and the Camassa-Holm equation [34]. In [35,37], LDG methods are designed for the Hunter-Saxton equation. There is a recent review paper on the LDG methods for high-order time-dependent partial differential equations [36], which provides more details. More general information about DG methods for elliptic, parabolic and hyperbolic partial differential equations can be found in the three special journal issues devoted to the DG method [7,8,12], as well as in the recent books and lecture notes [19,22,30,31].

The DG discretization results in an extremely local, element based discretization, which is beneficial for parallel computing and maintaining high order accuracy on un-

structured meshes. In particular, DG methods are well suited for *hp*-adaptation, which consists of local mesh refinement and/or the adjustment of the polynomial order in individual elements. They also have excellent provable nonlinear stability. The LDG method for the DP equation (1.1) that we design in this paper shares all these nice properties.

The paper is organized as follows. In Section 2, we present and analyze our LDG method for the DP equation (1.1). Section 3 contains numerical results to demonstrate the accuracy and capability of the methods. Concluding remarks are given in Section 4. Some of the more technical proofs of several lemmas are collected in the appendix.

2 The LDG methods for the DP equation

2.1 Notation

We denote the mesh of the domain Ω by $I_j=[x_{j-1/2},x_{j+1/2}]$, for $j=1,\cdots,J$. The center of the cell is $x_j=(x_{j-1/2}+x_{j+1/2})/2$ and the mesh size is denoted by $h_j=x_{j+1/2}-x_{j-1/2}$, with $h=\max_{1\le j\le J}h_j$ being the maximum mesh size. We assume the mesh is regular, namely the ratio between the maximum and the minimum mesh sizes stays bounded during mesh refinements. We define the piecewise-polynomial space V_h as the space of polynomials of the degree up to k in each cell I_j, i.e.,

$$V_h=\{v:\ v\in P^k(I_j),\quad \text{for}\ \ x\in I_j,\ \ j=1,\cdots,J\}.$$

Note that functions in V_h are allowed to have discontinuities across element interfaces.

The solution of the numerical scheme is denoted by u_h, which belongs to the finite element space V_h. We denote by $(u_h)^+_{j+1/2}$ and $(u_h)^-_{j+1/2}$ the values of u_h at $x_{j+1/2}$, from the right cell I_{j+1}, and from the left cell I_j, respectively. We use the usual notations $[u_h]=u_h^+-u_h^-$ and $\bar{u}_h=(u_h^++u_h^-)/2$ to denote the jump and the mean of the function u_h at each element boundary point, respectively.

2.2 The auxiliary variable and its equation

To obtain the L^2 bound on the solution u in terms of the L^2 norm of the initial data u_0, we need to introduce the auxiliary variable v which satisfies the following equation

$$4v-v_{xx}=u. \tag{2.1}$$

We assume the solution satisfies the periodic boundary conditions

$$u(x,t)=u(x+L,t),\qquad v(x,t)=v(x+L,t), \tag{2.2}$$

where L is the period in the x direction. Notice that the assumption of periodic boundary conditions is for simplicity only and is not essential: the method can be easily designed for non-periodic boundary conditions.

The motivation to the introduction of the variable v is from the energy $E_2(u)$ of the DP equation. One can use the variable v to get another form of the energy $E_2(u)$. It can be proved that the quantity v satisfies the energy stability [9]

$$\frac{d}{dt}\int_\Omega \left(2v^2+\frac{5}{2}(v_x)^2+\frac{1}{2}(v_{xx})^2\right)dx=0. \tag{2.3}$$

Thereby we can get the L^2 stability of u, i.e.,

$$\|u\|_{L^2(R)}\leqslant 2\sqrt{2}\|u_0\|_{L^2(R)}. \tag{2.4}$$

In order to prove the L^2 bound on the numerical solution u_h, we also need to introduce the LDG scheme for Eq. (2.1). We rewrite Eq. (2.1) as a first order system:

$$4v-z=u, \tag{2.5a}$$
$$z-w_x=0, \tag{2.5b}$$
$$w-v_x=0. \tag{2.5c}$$

The LDG method for Eq. (2.5) is formulated as follows: find v_h, w_h, $z_h\in V_h$, such that, for all test functions σ, ς, $\zeta\in V_h$,

$$\int_{I_j}4v_h\sigma dx-\int_{I_j}z_h\sigma dx=\int_{I_j}u_h\sigma dx, \tag{2.6a}$$
$$\int_{I_j}z_h\varsigma dx+\int_{I_j}w_h\varsigma_x dx-(\widehat{w}_h\varsigma^-)_{j+\frac{1}{2}}+(\widehat{w}_h\varsigma^+)_{j-\frac{1}{2}}=0, \tag{2.6b}$$
$$\int_{I_j}w_h\zeta dx+\int_{I_j}v_h\zeta_x dx-(\widehat{v}_h\zeta^-)_{j+\frac{1}{2}}+(\widehat{v}_h\zeta^+)_{j-\frac{1}{2}}=0. \tag{2.6c}$$

The "hat" terms in (2.6) in the cell boundary terms from integration by parts are the so-called "numerical fluxes", which are single valued functions defined on the edges and should be designed based on different guiding principles for different PDEs to ensure stability. For Eq. (2.6), we can take the simple choices of alternating fluxes such that

$$\widehat{w}_h=w_h^-,\qquad \widehat{v}_h=v_h^+, \tag{2.7}$$

where we have omitted the half-integer indices $j+1/2$ as all quantities in (2.7) are computed at the same points (i.e., the interfaces between the cells). We remark that the choice for the fluxes (2.7) is not unique. We can for example also choose the following numerical flux

$$\widehat{w}_h=w_h^+,\qquad \widehat{v}_h=v_h^-. \tag{2.8}$$

Remark 2.1. The LDG scheme (2.6) is only used for the proof of the L^2 stability of u_h. It does not need to be actually computed in the numerical algorithm.

In the following, we will give a Lemma which provides the energy stability relation for the schemes (2.6)-(2.7). This Lemma will be used to prove the energy stability for the different LDG schemes.

Lemma 2.1. *The solution to the schemes* (2.6)-(2.7) *satisfies the following equality*

$$\frac{d}{dt}\int_\Omega \Big(2v_h^2+\frac{5}{2}w_h^2+\frac{1}{2}z_h^2\Big)dx=\int_\Omega (u_h)_t(v_h-z_h)dx. \tag{2.9}$$

Proof. For Eq. (2.6), we first take the time derivative and choose the test functions $\sigma=v_h-z_h$, $\varsigma=v_h$ and $\zeta=4w_h$, then we get

$$\int_{I_j} 4(v_h)_t(v_h-z_h)dx-\int_{I_j}(z_h)_t(v_h-z_h)dx=\int_{I_j}(u_h)_t(v_h-z_h)dx, \tag{2.10a}$$

$$\int_{I_j}(z_h)_t v_h dx+\int_{I_j}(w_h)_t(v_h)_x dx-\big(\widehat{(w_h)_t}v_h^-\big)_{j+\frac{1}{2}}+\big(\widehat{(w_h)_t}v_h^+\big)_{j-\frac{1}{2}}=0, \tag{2.10b}$$

$$4\int_{I_j}(w_h)_t w_h dx+4\int_{I_j}(v_h)_t(w_h)_x dx-4\big(\widehat{(v_h)_t}w_h^-\big)_{j+\frac{1}{2}}+4\big(\widehat{(v_h)_t}w_h^+\big)_{j-\frac{1}{2}}=0. \tag{2.10c}$$

We can also choose the test functions $\varsigma=4(v_h)_t$, $\zeta=(w_h)_t$ in Eqs. (2.6b)-(2.6c) and obtain

$$4\int_{I_j} z_h(v_h)_t dx+4\int_{I_j} w_h((v_h)_t)_x dx-4\big(\widehat{w}_h(v_h)_t^-\big)_{j+\frac{1}{2}}+4\big(\widehat{w}_h(v_h)_t^+\big)_{j-\frac{1}{2}}=0, \tag{2.11a}$$

$$\int_{I_j} w_h(w_h)_t dx+\int_{I_j} v_h((w_h)_t)_x dx-\big(\widehat{v}_h(w_h)_t^-\big)_{j+\frac{1}{2}}+\big(\widehat{v}_h(w_h)_t^+\big)_{j-\frac{1}{2}}=0. \tag{2.11b}$$

Summing Eqs. (2.10a)-(2.11b) together, we can get

$$\int_{I_j}(4(v_h)_t v_h+5(w_h)_t w_h+(z_h)_t z_h)dx+\Psi_{j+\frac{1}{2}}-\Psi_{j-\frac{1}{2}}+\Theta_{j-\frac{1}{2}}=\int_{I_j}(u_h)_t(v_h-z_h)dx, \tag{2.12}$$

where the numerical entropy fluxes are given by

$$\Psi_{j+\frac{1}{2}}=\Big(4(w_h^-(v_h)_t^--(\widehat{w}_h(v_h)_t^-+\widehat{(v_h)_t}w_h^-))+v_h^-(w_h)_t^--(\widehat{v}_h(w_h)_t^-+\widehat{(w_h)_t}v_h^-)\Big)_{j+\frac{1}{2}},$$

and the extra term Θ is given by

$$\Theta_{j-\frac{1}{2}}=\Big(4(-[(v_h)_t w_h]+\widehat{(v_h)}_t[w_h]+\widehat{w}_h[(v_h)_t])-[(w_h)_t v_h]+\widehat{(w_h)}_t[v_h]+\widehat{v}_h[(w_h)_t]\Big)_{j-\frac{1}{2}}.$$

With the definition (2.7) of the numerical fluxes and after some algebraic manipulation, we easily obtain

$$-[(v_h)_t w_h]+\widehat{(v_h)}_t[w_h]+\widehat{w}_h[(v_h)_t]=0,$$
$$-[(w_h)_t v_h]+\widehat{(w_h)}_t[v_h]+\widehat{v}_h[(w_h)_t]=0.$$

Summing up Eq. (2.12) over j and taking into account the periodic boundary condition, we obtain Eq. (2.9). □

2.3 The LDG method (I)

In this section, we define our first LDG method for the DP equation (1.1), written in the following form

$$u_t - u_{txx} + 4f(u)_x = f(u)_{xxx}, \tag{2.13}$$

with an initial condition

$$u(x,0) = u_0(x), \tag{2.14}$$

where $f(u) = u^2/2$. We write Eq. (2.13) in the following form

$$u - u_{xx} = q, \tag{2.15a}$$
$$q_t + 4f(u)_x = f(u)_{xxx}. \tag{2.15b}$$

To define the local discontinuous Galerkin method, we further rewrite Eq. (2.15a) as a first order system:

$$u - r_x = q, \tag{2.16a}$$
$$r - u_x = 0. \tag{2.16b}$$

The LDG method for Eq. (2.16a), where q is assumed known and we would want to solve for u, is formulated as follows: find u_h, $r_h \in V_h$, such that, for all test functions ρ, $\phi \in V_h$,

$$\int_{I_j} u_h \rho dx + \int_{I_j} r_h \rho_x dx - (\widehat{r}_h \rho^-)_{j+\frac{1}{2}} + (\widehat{r}_h \rho^+)_{j-\frac{1}{2}} = \int_{I_j} q_h \rho dx, \tag{2.17a}$$
$$\int_{I_j} r_h \phi dx + \int_{I_j} u_h \phi_x dx - (\widehat{u}_h \phi^-)_{j+\frac{1}{2}} + (\widehat{u}_h \phi^+)_{j-\frac{1}{2}} = 0. \tag{2.17b}$$

Corresponding to the numerical flux (2.7), we can take the simple choices such that

$$\widehat{r}_h = r_h^-, \qquad \widehat{u}_h = u_h^+. \tag{2.18}$$

For Eq. (2.15b), we can also rewrite it into a first order system:

$$q_t + 4s - p_x = 0, \tag{2.19a}$$
$$p - s_x = 0, \tag{2.19b}$$
$$s - f(u)_x = 0. \tag{2.19c}$$

Now we can define a local discontinuous Galerkin method to the equations in (2.19), resulting in the following scheme: find q_h, p_h, $s_h \in V_h$, such that, for all test functions φ, ψ, $\eta \in V_h$,

$$\int_{I_j} (q_h)_t \varphi dx + \int_{I_j} 4s_h \varphi dx + \int_{I_j} p_h \varphi_x dx - (\widehat{p}_h \varphi^-)_{j+\frac{1}{2}} + (\widehat{p}_h \varphi^+)_{j-\frac{1}{2}} = 0, \tag{2.20a}$$
$$\int_{I_j} p_h \psi dx + \int_{I_j} s_h \psi_x dx - (\widehat{s_h} \psi^-)_{j+\frac{1}{2}} + (\widehat{s_h} \psi^+)_{j-\frac{1}{2}} = 0, \tag{2.20b}$$
$$\int_{I_j} s_h \eta dx + \int_{I_j} f(u_h) \eta_x dx - (\widehat{f} \eta^-)_{j+\frac{1}{2}} + (\widehat{f} \eta^+)_{j-\frac{1}{2}} = 0. \tag{2.20c}$$

The numerical fluxes in Eqs. (2.20) are chosen as

$$\widehat{p}_h = p_h^-, \qquad \widehat{s}_h = s_h^+, \tag{2.21}$$

and $\widehat{f}(u_h^-, u_h^+)$ is a monotone flux for solving conservation laws, i.e., it is Lipschitz continuous in both arguments, consistent ($\widehat{f}(u_h, u_h) = f(u_h)$), non-decreasing in the first argument and non-increasing in the second argument. Examples of monotone fluxes which are suitable for discontinuous Galerkin methods can be found in, e.g., [4]. We could for example use the simple Lax-Friedrichs flux

$$\widehat{f}(u_h^-, u_h^+) = \frac{1}{2}\left(f(u_h^-) + f(u_h^+) - \varepsilon(u_h^+ - u_h^-)\right), \qquad \varepsilon = \max|f'(u_h)|,$$

where the maximum is taken over a relevant range of u_h. This Lax-Friedrichs flux is used in the numerical experiments in next section. The definition of the algorithm is now complete.

We remark that the choice for the fluxes (2.18) and (2.21) is not unique. We can for example also choose the following numerical flux

$$\widehat{r}_h = r_h^+, \quad \widehat{u}_h = u_h^-, \quad \widehat{p}_h = p_h^+, \quad \widehat{s}_h = s_h^-, \tag{2.22}$$

which is corresponding to the numerical flux (2.8).

Algorithm flowchart (I)

In this section, we give the details related to the implementation of the method.

• Given the solution u_h at time level n, we first obtain q_h from Eqs. (2.17)-(2.18) in the following matrix form

$$\boldsymbol{q}_h = \mathbf{A}\boldsymbol{u}_h, \tag{2.23}$$

where $\boldsymbol{q}_h$ and $\boldsymbol{u}_h$ are the vectors containing the degrees of freedom for q_h and u_h, respectively.

• From (2.20)-(2.21), we obtain the LDG discretization of the residual $4f(u)_x - f(u)_{xxx}$ in the following vector form

$$(\boldsymbol{q}_h)_t = \mathbf{res}(\boldsymbol{u}_h). \tag{2.24}$$

• We then combine (2.23) and (2.24) to obtain

$$\mathbf{A}(\boldsymbol{u}_h)_t = \mathbf{res}(\boldsymbol{u}_h). \tag{2.25}$$

• We use a time discretization method to solve

$$(\boldsymbol{u}_h)_t = \mathbf{A}^{-1}\mathbf{res}(\boldsymbol{u}_h). \tag{2.26}$$

This step involves a linear solver with the matrix **A**. We perform a *LU* decomposition for **A** at the beginning and use it for all time steps. Any standard ODE solvers can be used here, for example the Runge-Kutta methods.

The LDG matrix **A** is a sparse block matrix, hence its multiplication with vectors and a linear solver involving it as the coefficient matrix can be implemented efficiently.

Proposition 2.1. (Energy stability of the solution v_h) The solution to the schemes (2.17)-(2.18) and (2.20)-(2.21) satisfies the stability property

$$\frac{d}{dt}\int_\Omega \Big(2v_h^2+\frac{5}{2}w_h^2+\frac{1}{2}z_h^2\Big)dx\le 0. \tag{2.27}$$

Proof. For Eqs. (2.17), we first take the time derivative and take the test functions $\rho=v_h$ and $\phi=-w_h$, then we get

$$\int_{I_j}(u_h)_t v_h dx+\int_{I_j}(r_h)_t(v_h)_x dx-\big(\widehat{(r_h)_t}v_h^-\big)_{j+\frac{1}{2}}+\big(\widehat{(r_h)_t}v_h^+\big)_{j-\frac{1}{2}}=\int_{I_j}(q_h)_t v_h dx, \tag{2.28a}$$

$$-\int_{I_j}(r_h)_t w_h dx-\int_{I_j}(u_h)_t(w_h)_x dx+\big(\widehat{(u_h)_t}w_h^-\big)_{j+\frac{1}{2}}-\big(\widehat{(u_h)_t}w_h^+\big)_{j-\frac{1}{2}}=0. \tag{2.28b}$$

We also choose the test function in Eqs. (2.20) and (2.6) in the following

$$\varphi=v_h,\quad \psi=-w_h,\quad \eta=-u_h,\quad \sigma=-s_h,\quad \varsigma=-(u_h)_t-s_h,\quad \zeta=p_h+(r_h)_t,$$

and sum up with Eqs. (2.28a) and (2.28b). Taking $F(u_h)=\int^{u_h} f(\tau)d\tau$, then we obtain

$$\int_{I_j}(u_h)_t(v_h-z_h)dx+\Upsilon_{j+\frac{1}{2}}-\Upsilon_{j-\frac{1}{2}}+\Lambda_{j-\frac{1}{2}}=0, \tag{2.29}$$

where the numerical entropy fluxes are given by

$$\begin{aligned}\Upsilon_{j+\frac{1}{2}}=\Big(&-F(u_h^-)+\widehat{f}u_h^- -(w_h^-((u_h)_t+s_h)^- -(\widehat{w}_h((u_h)_t+s_h)^- +(\widehat{(u_h)_t}+\widehat{s_h})w_h^-))\\ &+v_h^-((r_h)_t+p_h)^- -(\widehat{v}_h((r_h)_t+p_h)^- +(\widehat{(r_h)_t}+\widehat{p_h})v_h^-)\Big)_{j+\frac{1}{2}},\end{aligned}$$

and the extra term Λ is given by

$$\begin{aligned}\Lambda_{j-\frac{1}{2}}=\Big(&[F(u_h)]-\widehat{f}[u_h]-(-[((u_h)_t+s_h)w_h]+(\widehat{(u_h)}_t+\widehat{s_h})[w_h]+\widehat{w}_h[(u_h)_t+s_h])\\ &-[((r_h)_t+p_h)v_h]+(\widehat{(r_h)}_t+\widehat{p_h})[v_h]+\widehat{v}_h[(r_h)_t+p_h]\Big)_{j-\frac{1}{2}}.\end{aligned}$$

With the definition (2.7), (2.18) and (2.21) of the numerical fluxes and after some algebraic manipulation, we easily obtain

$$\begin{aligned}&-[((u_h)_t+s_h)w_h]+(\widehat{(u_h)}_t+\widehat{s_h})[w_h]+\widehat{w}_h[(u_h)_t+s_h]=0,\\ &-[((r_h)_t+p_h)v_h]+(\widehat{(r_h)}_t+\widehat{p_h})[v_h]+\widehat{v}_h[(r_h)_t+p_h]=0,\end{aligned}$$

and hence

$$\Lambda_{j-\frac{1}{2}} = \left([F(u_h)] - \widehat{f}[u_h]\right)_{j-\frac{1}{2}} \geq 0,$$

where the last inequality follows from the monotonicity of the flux

$$[F(u_h)] - \widehat{f}[u_h] = \int_{u_h^-}^{u_h^+} \left(f(s) - \widehat{f}(u_h^-, u_h^+)\right) ds \geq 0.$$

Summing up Eq. (2.29) over j and taking into account the periodic boundary condition, we obtain

$$\int_\Omega (u_h)_t (v_h - z_h) dx \leq 0.$$

Combining with the results in Lemma 2.1, we obtain the energy stability in (2.27). □

2.4 The LDG method (II)

Eq. (2.13) is formally equivalent to the system

$$u_t + f(u)_x + p = 0, \tag{2.30a}$$
$$p - p_{xx} = 3f(u)_x. \tag{2.30b}$$

To define another local discontinuous Galerkin method, we further rewrite Eq. (2.30a) as a first order system:

$$u_t + q + p = 0, \tag{2.31a}$$
$$p - s_x = 3q, \tag{2.31b}$$
$$s - p_x = 0, \tag{2.31c}$$
$$q - f(u)_x = 0. \tag{2.31d}$$

The LDG method for Eq. (2.31) is formulated as follows: find u_h, s_h, p_h, $q_h \in V_h$, such that, for all test functions φ, ψ, $\eta \in V_h$,

$$\int_{I_j} (u_h)_t \varphi dx + \int_{I_j} (q_h + p_h)\varphi dx = 0, \tag{2.32a}$$
$$\int_{I_j} p_h \psi dx + \int_{I_j} s_h \psi_x dx - (\widehat{s}_h \psi^-)_{j+\frac{1}{2}} + (\widehat{s}_h \psi^+)_{j-\frac{1}{2}} = 3\int_{I_j} q_h \psi dx, \tag{2.32b}$$
$$\int_{I_j} s_h \eta dx + \int_{I_j} p_h \eta_x dx - (\widehat{p}_h \eta^-)_{j+\frac{1}{2}} + (\widehat{p}_h \eta^+)_{j-\frac{1}{2}} = 0, \tag{2.32c}$$
$$\int_{I_j} q_h \rho dx + \int_{I_j} f(u_h)\rho_x dx - (\widehat{f}\rho^-)_{j+\frac{1}{2}} + (\widehat{f}\rho^+)_{j-\frac{1}{2}} = 0. \tag{2.32d}$$

Corresponding to the numerical flux (2.7), the numerical fluxes in Eq. (2.32) are chosen as

$$\widehat{p}_h = p_h^-, \qquad \widehat{s}_h = s_h^+. \tag{2.33}$$

Here $\widehat{f}(u_h^-, u_h^+)$ is a monotone flux for solving conservation laws. The definition of the algorithm is now complete.

We remark that the choice for the fluxes (2.33) is not unique. We can for example also choose the following numerical flux

$$\widehat{p}_h = p_h^+, \qquad \widehat{s}_h = s_h^-, \tag{2.34}$$

which is corresponding to the numerical flux (2.8).

Algorithm flowchart (II)

In this section, we give details related to the implementation of the method.

• Given the solution u_h at time level n, we first solve Eq. (2.32d) to get $\boldsymbol{q}_h$.

$$\boldsymbol{q}_h = \mathbf{res}(\boldsymbol{u}_h). \tag{2.35}$$

• From (2.32b), (2.32c) and (2.33), we obtain the following matrix form

$$\mathbf{A}\boldsymbol{p}_h = 3\boldsymbol{q}_h. \tag{2.36}$$

This step involves a linear solver with the matrix $\mathbf{A}$. Then we get

$$\boldsymbol{p}_h = 3\mathbf{A}^{-1}\boldsymbol{q}_h. \tag{2.37}$$

• Using the solution $\boldsymbol{q}_h$, $\boldsymbol{p}_h$ of (2.35) and (2.37) to computing discretization of the residual in (2.32a), then we obtain

$$(\boldsymbol{u}_h)_t = \boldsymbol{q}_h + \boldsymbol{p}_h. \tag{2.38}$$

Any standard ODE solvers can be used here, for example the Runge-Kutta methods.

Proposition 2.2. (Energy stability of solution v_h) The solution to the schemes (2.32)-(2.33) satisfies the stability property

$$\frac{d}{dt}\int_\Omega \left(2v_h^2 + \frac{5}{2}w_h^2 + \frac{1}{2}z_h^2\right)dx \le 0. \tag{2.39}$$

Proof. Since (2.32) and (2.6) hold for any test functions in V_h, we can choose

$$\varphi = v_h - z_h, \quad \psi = -v_h, \quad \eta = w_h, \quad \rho = -u_h, \quad \sigma = -q_h, \quad \varsigma = p_h, \quad \zeta = -s_h,$$

and sum up the equations. Taking $F(u_h)=\int^{u_h} f(\tau)d\tau$, then we obtain

$$\int_{I_j}(u_h)_t(v_h-z_h)dx+\Phi_{j+\frac{1}{2}}-\Phi_{j-\frac{1}{2}}+\Xi_{j-\frac{1}{2}}=0, \tag{2.40}$$

where the numerical entropy fluxes are given by

$$\Phi_{j+\frac{1}{2}}=\Big(-F(u_h^-)+\widehat{f}u_h^-+(w_h^-p_h^--(\widehat{w}_hp_h^-+\widehat{p}_hw_h^-))-(v_h^-s_h^--(\widehat{v}_hs_h^-+\widehat{s}_hv_h^-))\Big)_{j+\frac{1}{2}},$$

and the extra term Ξ is given by

$$\Xi_{j-\frac{1}{2}}=\Big([F(u_h)]-\widehat{f}[u_h]+(-[p_hw_h]+\widehat{p_h}[w_h]+\widehat{w}_h[p_h])-(-[s_hv_h]+\widehat{(s_h)}[v_h]+\widehat{v}_h[s_h])\Big)_{j-\frac{1}{2}}.$$

With the definition (2.7) and (2.33) of the numerical fluxes and after some algebraic manipulation, we easily obtain

$$\begin{aligned}&-[p_hw_h]+\widehat{p}_h[w_h]+\widehat{w}_h[p_h])=0,\\&-[s_hv_h]+\widehat{s}_h[v_h]+\widehat{v}_h[s_h]=0,\end{aligned}$$

and hence

$$\Xi_{j-\frac{1}{2}}=\big([F(u_h)]-\widehat{f}[u_h]\big)_{j-\frac{1}{2}}\geq 0,$$

where the last inequality follows from the monotonicity of the flux

$$[F(u_h)]-\widehat{f}[u_h]=\int_{u_h^-}^{u_h^+}(f(s)-\widehat{f}(u_h^-,u_h^+))ds\geq 0.$$

Summing up Eq. (2.40) over j and taking into account the periodic boundary condition, we obtain

$$\int_\Omega(u_h)_t(v_h-z_h)dx\leq 0.$$

Combining with the results in Lemma 2.1, we can get energy stability in (2.39). □

2.5 L^2 stability of solution u_h

Proposition 2.3. (L^2 stability) The solutions to the LDG Schemes (I) and (II) both satisfy the stability property

$$\|u_h\|_{L^2(\Omega)}\leq 2\sqrt{2}\|u_0\|_{L^2(\Omega)}. \tag{2.41}$$

Proof. From Eq. (2.6a), we can easily obtain

$$\begin{aligned}\int_\Omega u_h^2 dx &= \int_\Omega (4v_h - z_h)^2 dx \le 2\int_\Omega (16v_h^2 + z_h^2) dx \\ &\le 16\int_\Omega \Big(2v_h^2 + \frac{5}{2}w_h^2 + \frac{1}{2}z_h^2\Big) dx.\end{aligned}$$

By using the stability results for v_h of Scheme (I) or (II), we have

$$\int_\Omega u_h^2 dx \le 16\int_\Omega \Big(2v_0^2 + \frac{5}{2}w_0^2 + \frac{1}{2}z_0^2\Big) dx. \tag{2.42}$$

In Eqs. (2.6b) and (2.6c), we choose the test function $\varsigma = v_h$, $\zeta = w_h$. By the definition of numerical flux (2.7) and some algebraic manipulation, we easily obtain

$$\int_\Omega z_h v_h dx = -\int_\Omega w_h^2 dx. \tag{2.43}$$

On the other hand, we also have

$$\int_\Omega u_h^2 dx = \int_\Omega (16v_h^2 - 8v_h z_h + z_h^2) dx = \int_\Omega (16v_h^2 + 8w_h^2 + z_h^2) dx \ge \int_\Omega (4v_h^2 + 5w_h^2 + z_h^2) dx.$$

For $t = 0$, we will have

$$\int_\Omega u_0^2 dx \ge \int_\Omega (4v_0^2 + 5w_0^2 + z_0^2) dx. \tag{2.44}$$

Combining (2.42) and (2.44), we get

$$\int_\Omega u_h^2 dx \le 8\int_\Omega u_0^2 dx,$$

which implies (2.41). □

2.6 Total variation bounded property for the P^0 case

In this section, we will discuss the total variation bounded property for the P^0 case in the uniform grid. We denote the mesh size by h and the time step by Δt. The cell average of the solution u_h is denoted as

$$u_j = \frac{1}{h}\int_{I_j} u_h dx.$$

We also denote

$$\mathcal{I}u_j = u_j, \qquad \Delta_+ u_j = u_{j+1} - u_j, \qquad \Delta_- u_j = u_j - u_{j-1}.$$

Now we can get the scheme for the P^0 case:

- Scheme (I)

$$\frac{d}{dt}\Big(\mathcal{I}-\frac{1}{h^2}\Delta_+\Delta_-\Big)u_j+4\frac{\widehat{f}_{j+\frac{1}{2}}-\widehat{f}_{j-\frac{1}{2}}}{h}-\frac{\widehat{f}_{j+\frac{3}{2}}-3\widehat{f}_{j+\frac{1}{2}}+3\widehat{f}_{j-\frac{1}{2}}-\widehat{f}_{j-\frac{3}{2}}}{\Delta x^3}=0. \tag{2.45}$$

- Scheme (II)

$$\frac{du_j}{dt}+\frac{\widehat{f}_{j+\frac{1}{2}}-\widehat{f}_{j-\frac{1}{2}}}{h}+p_j=0, \tag{2.46a}$$

$$\Big(\mathcal{I}-\frac{1}{h^2}\Delta_+\Delta_-\Big)p_j=3\frac{\widehat{f}_{j+\frac{1}{2}}-\widehat{f}_{j-\frac{1}{2}}}{h}. \tag{2.46b}$$

Eq. (2.46b) can be written into the matrix form

$$\mathbf{A}\boldsymbol{p}_h=\mathbf{res}(\boldsymbol{u}_h), \tag{2.47}$$

where the matrix $\mathbf{A}$ is a tridiagonal matrix in the following form

$$\mathbf{A}=\begin{pmatrix} 1+2a & -a & 0 & \cdots & 0 & -a \\ -a & 1+2a & -a & 0 & \cdots & 0 \\ 0 & -a & 1+2a & -a & 0 & 0 \\ \vdots & \vdots & \ddots & \ddots & \ddots & \vdots \\ 0 & \cdots & 0 & -a & 1+2a & -a \\ -a & 0 & \cdots & 0 & -a & 1+2a \end{pmatrix}, \qquad a=\frac{1}{h^2}, \tag{2.48}$$

and $\boldsymbol{p}_h$, $\boldsymbol{u}_h$ are the vectors containing $\{p_j\}$, $\{u_j\}$, respectively.

Remark 2.2. For Eq. (2.45), we can rewrite it as

$$\frac{d}{dt}\Big(\mathcal{I}-\frac{1}{h^2}\Delta_+\Delta_-\Big)u_j+3\frac{\widehat{f}_{j+\frac{1}{2}}-\widehat{f}_{j-\frac{1}{2}}}{h}+\Big(\mathcal{I}-\frac{1}{h^2}\Delta_+\Delta_-\Big)\frac{\widehat{f}_{j+\frac{1}{2}}-\widehat{f}_{j-\frac{1}{2}}}{h}=0. \tag{2.49}$$

After taking the inverse of matrix $\mathbf{A}$, we can see that the scheme (2.49) and (2.46) are the same. In the following, we only discuss the scheme (2.46).

Lemma 2.2. (Property of $\mathbf{A}^{-1}$) *The inverse of the matrix* $\mathbf{A}$ *can be written as*

$$\mathbf{A}^{-1}=\begin{pmatrix} \alpha_1 & \alpha_2 & \cdots & \alpha_{J-1} & \alpha_J \\ \alpha_J & \alpha_1 & \alpha_2 & \cdots & \alpha_{J-1} \\ \vdots & \vdots & \ddots & \vdots & \vdots \\ \alpha_3 & \cdots & \alpha_J & \alpha_1 & \alpha_2 \\ \alpha_2 & \cdots & \alpha_{J-1} & \alpha_J & \alpha_1 \end{pmatrix}, \tag{2.50}$$

where $\{\alpha_j\}$ *satisfy the following properties*

$$|\alpha_j-\alpha_{j+1}|<\frac{1}{2}h^2,\quad j=1,\cdots,J-1, \tag{2.51a}$$

$$0\leqslant\alpha_1-\alpha_J<\frac{1}{2}h^2. \tag{2.51b}$$

Proof. The proof of this lemma will be given in the appendix. □

After inverting the matrix **A** in (2.46b), we can get

$$p_j=3\sum_{i=1}^{J}\alpha_i\frac{\widehat{f}_{j+i+\frac{1}{2}}-\widehat{f}_{j+i-\frac{1}{2}}}{h}. \tag{2.52}$$

Now the scheme (2.46a) becomes

$$\frac{du_j}{dt}+\frac{\widehat{f}_{j+\frac{1}{2}}-\widehat{f}_{j-\frac{1}{2}}}{h}+3\sum_{i=1}^{J}\alpha_i\frac{\widehat{f}_{j+i+\frac{1}{2}}-\widehat{f}_{j+i-\frac{1}{2}}}{h}=0. \tag{2.53}$$

For simplicity, we will only consider the forward Euler time discretization of the semi-discrete scheme (2.52). Now we will get the fully discretized scheme

$$u_j^{n+1}=u_j^n-\lambda\big(\widehat{f}^n_{j+\frac{1}{2}}-\widehat{f}^n_{j-\frac{1}{2}}\big)-3\lambda\sum_{i=1}^{J}\alpha_i\big(\widehat{f}^n_{j+i+\frac{1}{2}}-\widehat{f}^n_{j+i-\frac{1}{2}}\big), \tag{2.54}$$

where $\lambda=\Delta t/h$. With a simple calculation, we can get

$$-\lambda(\widehat{f}^n_{j+\frac{1}{2}}-\widehat{f}^n_{j-\frac{1}{2}})=-\lambda\frac{\widehat{f}(u_j^n,u_{j+1}^n)-\widehat{f}(u_j^n,u_j^n)}{\Delta_+u_j^n}\Delta_+u_j^n-\lambda\frac{\widehat{f}(u_j^n,u_j^n)-\widehat{f}(u_{j-1}^n,u_j^n)}{\Delta_-u_j^n}\Delta_-u_j^n.$$

Denoting

$$\mathcal{C}_{j+\frac{1}{2}}=-\lambda\frac{\widehat{f}(u_j^n,u_{j+1}^n)-\widehat{f}(u_j^n,u_j^n)}{\Delta_+u_j^n},\qquad D_{j-\frac{1}{2}}=\lambda\frac{\widehat{f}(u_j^n,u_j^n)-\widehat{f}(u_{j-1}^n,u_j^n)}{\Delta_-u_j^n},$$

we have

$$0\leqslant\mathcal{C}_{j+\frac{1}{2}}\leqslant\lambda L_2,\qquad 0\leqslant D_{j+\frac{1}{2}}\leqslant\lambda L_1, \tag{2.55}$$

where we have used the monotonicity and Lipschitz continuity of flux $\widehat{f}$, which is non-decreasing in the first argument and non-increasing in the second argument. L_1 and L_2 are the Lipschitz constants of $\widehat{f}$ with respect to its first and second arguments, respectively. If we choose the time step so that

$$\lambda\leqslant\frac{1}{L_1+L_2}, \tag{2.56}$$

we also have

$$1-\mathcal{C}_{j+\frac{1}{2}}-D_{j+\frac{1}{2}}\geqslant 0. \tag{2.57}$$

Since we have

$$-\lambda\left(\widehat{f}^n_{j+\frac{1}{2}}-\widehat{f}^n_{j-\frac{1}{2}}\right)=\mathcal{C}_{j+\frac{1}{2}}\Delta_+u^n_j-D_{j-\frac{1}{2}}\Delta_-u^n_j, \tag{2.58}$$

we can rewrite Eq. (2.54) into the following form

$$u^{n+1}_j=u^n_j+\mathcal{C}_{j+\frac{1}{2}}\Delta_+u^n_j-D_{j-\frac{1}{2}}\Delta_-u^n_j+3\sum_{i=1}^{J}\alpha_i\left(\mathcal{C}_{j+i+\frac{1}{2}}\Delta_+u^n_{j+i}-D_{j+i-\frac{1}{2}}\Delta_-u^n_{j+i}\right). \tag{2.59}$$

Taking the forward difference operation Δ_+ on (2.59), we have

$$\begin{aligned}\Delta_+u^{n+1}_j=&(1-\mathcal{C}_{j+\frac{1}{2}}-D_{j+\frac{1}{2}})\Delta_+u^n_j+\mathcal{C}_{j+\frac{3}{2}}\Delta_+u^n_{j+1}+D_{j-\frac{1}{2}}\Delta_-u^n_j+3\sum_{i=1}^{J}\alpha_i\mathcal{C}_{j+i+\frac{3}{2}}\Delta_+u^n_{j+i+1}\\&-3\sum_{i=1}^{J}\alpha_i\mathcal{C}_{j+i+\frac{1}{2}}\Delta_+u^n_{j+i}-3\sum_{i=1}^{J}\alpha_iD_{j+i+\frac{1}{2}}\Delta_-u^n_{j+i+1}+3\sum_{i=1}^{J}\alpha_iD_{j+i-\frac{1}{2}}\Delta_-u^n_{j+i}.\end{aligned}$$

Using the property (2.55), (2.57), (2.51a) and periodicity of the solution, we can obtain

$$\begin{aligned}\sum_{j=1}^{J}|\Delta_+u^{n+1}_j|\leqslant&\sum_{j=1}^{J}(1-\mathcal{C}_{j+\frac{1}{2}}-D_{j+\frac{1}{2}})|\Delta_+u^n_j|+\sum_{j=1}^{J}\mathcal{C}_{j+\frac{3}{2}}|\Delta_+u^n_{j+1}|+\sum_{j=1}^{J}D_{j-\frac{1}{2}}|\Delta_-u^n_j|\\&+3\sum_{j=1}^{J}\Big|\sum_{i=1}^{J}\alpha_i\mathcal{C}_{j+i+\frac{3}{2}}\Delta_+u^n_{j+i+1}-\sum_{i=1}^{J}\alpha_i\mathcal{C}_{j+i+\frac{1}{2}}\Delta_+u^n_{j+i}\Big|\\&+3\sum_{j=1}^{J}\Big|\sum_{i=1}^{J}\alpha_iD_{j+i-\frac{1}{2}}\Delta_-u^n_{j+i}-\sum_{i=1}^{J}\alpha_iD_{j+i+\frac{1}{2}}\Delta_-u^n_{j+i+1}\Big|\\=&\sum_{j=1}^{J}(1-\mathcal{C}_{j+\frac{1}{2}}-D_{j+\frac{1}{2}})|\Delta_+u^n_j|+\sum_{j=1}^{J}\mathcal{C}_{j+\frac{1}{2}}|\Delta_+u^n_j|+\sum_{j=1}^{J}D_{j+\frac{1}{2}}|\Delta_+u^n_j|\\&+3\sum_{j=1}^{J}\Big|\sum_{i=1}^{J}(\alpha_i-\alpha_{i-1})\mathcal{C}_{j+i+\frac{1}{2}}\Delta_+u^n_{j+i}\Big|+3\sum_{j=1}^{J}\Big|\sum_{i=1}^{J}(\alpha_{i+1}-\alpha_i)D_{j+i+\frac{1}{2}}\Delta_+u^n_{j+i}\Big|\\\leqslant&\sum_{j=1}^{J}|\Delta_+u^n_j|+3\sum_{j=1}^{J}\sum_{i=1}^{J}\left(|\alpha_i-\alpha_{i-1}|\mathcal{C}_{j+i+\frac{1}{2}}+|\alpha_{i+1}-\alpha_i|D_{j+i+\frac{1}{2}}\right)|\Delta_+u^n_{j+i}|\\\leqslant&\sum_{j=1}^{J}|\Delta_+u^n_j|+\frac{3}{2}\sum_{j=1}^{J}\sum_{i=1}^{J}h^2(L_1+L_2)|\Delta_+u^n_{j+i}|\\=&\sum_{j=1}^{J}|\Delta_+u^n_j|+\frac{3}{2}(L_1+L_2)\sum_{j=1}^{J}h^2J|\Delta_+u^n_j|\\\leqslant&\sum_{j=1}^{J}|\Delta_+u^n_j|+C\Delta t\sum_{j=1}^{J}|\Delta_+u^n_j|.\end{aligned}$$

If we denote the "total variation in the means" semi-norm, or TVM as

$$\mathrm{TVM}(u_h)=\sum_{j=1}^{J}|\Delta_+ u_j|,$$

which for the piecewise constant case under study is just the standard bounded variation semi-norm, then we have

$$\mathrm{TVM}(u_h^{n+1})\leqslant(1+C\Delta t)\mathrm{TVM}(u_h^n)\leqslant(1+C\Delta t)^{n+1}\mathrm{TVM}(u^0)\leqslant\exp(CT)\mathrm{TVM}(u^0).$$

Now we have the following proposition.

Proposition 2.4. For the periodic boundary conditions, the solutions of the Schemes (I) and (II) for the P^0 case with Euler forward time discretization is total variation bounded, that is

$$\mathrm{TVM}(u_h^n)\leqslant\exp(CT)\mathrm{TVM}(u^0).$$

Remark 2.3. Even though Proposition 2.4 is proved only for the first order Euler forward time discretization, the special total variation diminishing (TVD) Runge-Kutta time discretization [32] allows us to obtain the same result for the high order in time fully discretized scheme. However, this is not necessary if the spatial accuracy is only first order.

2.7 Comparison of the two schemes

In this section, we give some comments on the comparison of the two proposed LDG schemes.

• The Scheme (I) is based on the dispersive form Eqs. (2.15a)-(2.15b) and the Scheme (II) is based on the hyperbolic-elliptic form Eq. (2.30a).

• The L^2 stability for the general case of both schemes can be proved.

• TVB property for the P^0 case of both schemes can be proved.

• For the computational cost, the Scheme (II) is more efficient than the Scheme (I) because the Scheme (I) has one more Eq. (2.20b) to compute. But the difference of the real computational time is small.

• The computational performance of the two schemes is almost the same. The results are shown in Section 3.

3 Numerical results

In this section we provide numerical examples to illustrate the accuracy and capability of the proposed methods. Time discretization is by the third order explicit TVD Runge-Kutta method in [32]. The time step for both schemes is $\Delta t=Ch$, where the constant C

depends on the cfl number and $\max_\Omega|u|$. This is not the most efficient method for the time discretization to our LDG scheme. However, we will not address the issue of time discretization efficiency in this paper. We have verified with the aid of successive mesh refinements, that in all cases, the results shown are numerically convergent. We will give the numerical test results for the DP equation

$$u_t - u_{txx} + 4f(u)_x = f(u)_{xxx}, \tag{3.1}$$

with $f(u) = u^2/2$ for different initial conditions. We choose the computational domain large enough so that the solution is small enough at the boundary of the domain for the periodic boundary condition to hold approximately at the level of truncation errors.

Example 3.1. Accuracy test

The peakon solutions of the DP equation (3.1) are well known. The peaked traveling wave solution is

$$u(x,t) = ce^{-|x-ct|}, \tag{3.2}$$

where c is the wave speed. We give the accuracy test with $c = 0.25$. The accuracy is measured in smooth parts of the solution, 1/10 of the computational domain away from the peak. The L^2 and L^∞ errors and the numerical orders of accuracy for u at time $t = 1$ with uniform meshes in $[-25,25]$ are contained in Table 1. We can see that the methods

Table 1: Accuracy test for the DP equation (3.1) with the exact solution (3.2). Periodic boundary condition. $c = 0.25$. Uniform meshes with N cells at time $t = 1$.

		Scheme (I)				Scheme (II)			
	N	L^2 error	order	L^∞ error	order	L^2 error	order	L^∞ error	order
p^0	20	6.62E-03	–	6.84E-02	–	6.62E-03	–	6.84E-02	–
	40	1.98E-03	1.74	2.18E-02	1.65	1.98E-03	1.74	2.18E-02	1.65
	80	8.56E-04	1.21	1.02E-02	1.09	8.56E-04	1.21	1.02E-02	1.09
	160	4.76E-04	0.85	6.39E-03	0.68	4.76E-04	0.85	6.39E-03	0.68
p^1	20	2.31E-03	–	3.19E-02	–	2.31E-03	–	3.19E-02	–
	40	1.73E-04	3.74	2.42E-03	3.71	1.73E-04	3.74	2.43E-03	3.71
	80	3.92E-05	2.14	5.31E-04	2.19	3.92E-05	2.14	5.31E-04	2.19
	160	1.08E-05	1.86	1.88E-04	1.50	1.08E-05	1.86	1.88E-04	1.50
p^2	20	3.90E-04	–	6.61E-03	–	3.90E-04	–	6.61E-03	–
	40	3.35E-05	3.54	5.25E-04	3.93	3.35E-05	3.54	4.33E-04	3.93
	80	4.07E-06	3.04	5.25E-05	3.04	4.07E-06	3.04	5.25E-05	3.04
	160	5.77E-07	2.82	7.13E-06	2.88	5.77E-07	2.82	7.13E-06	2.88
p^3	10	1.49E-03	–	1.77E-02	–	1.49E-03	–	1.77E-02	–
	20	1.51E-04	3.30	2.69E-03	2.72	1.51E-04	3.30	2.69E-03	2.72
	40	7.64E-06	4.30	1.32E-04	4.35	7.64E-06	4.31	1.32E-04	4.36
	80	1.60E-07	5.58	2.13E-06	5.95	1.60E-07	5.58	2.13E-06	5.95
p^4	10	7.07E-03	–	7.09E-02	–	7.07E-03	–	7.09E-02	–
	20	1.72E-04	5.36	2.75E-03	4.69	1.72E-04	5.36	2.76E-03	4.68
	40	4.68E-06	5.20	8.45E-05	5.02	4.68E-06	5.20	8.45E-05	5.03
	80	8.30E-08	5.82	1.31E-06	6.01	8.30E-08	5.82	1.31E-06	6.01

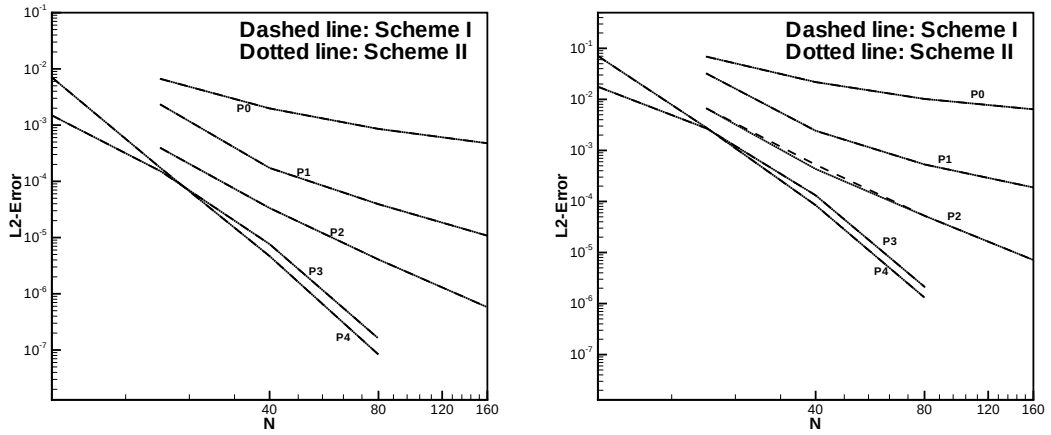

(a) L^2 error (b) L^∞ error

Figure 1: Error comparison of two schemes for the DP equation (3.1) with the exact solution (3.2). Periodic boundary condition. $c=0.25$. Uniform meshes with N cells at time $t=1$.

with P^k elements generally gives optimal (k+1)-th order of accuracy for u in both norms. In Fig. 1, We show the comparison of the accuracy order of both schemes. The errors are drawn on a log-log scale so the slope of the error lines indicates the expected order of convergence. The error results are almost the same for both of the schemes.

Example 3.2. Peakon solution

In this example, we present the wave propagation of the peakon solution (3.2) and anti-peakon solution

$$u(x,t)=-ce^{-|x+ct|}. \tag{3.3}$$

We present the wave propagation for the DP equation with the parameter $c=1$. The computational domain is $[-40,40]$. In Figs. 2 and 3, the peakon and anti-peakon profile at $t=4$, 8, 12 and 16 are shown. The lack of smoothness at the peak of peakon introduces high-frequency dispersive errors into the calculation and may cause numerical oscillations near the peak when the solution is under-resolved. In our computation of the LDG method, we use the P^4 element with $N=228$ cells to resolve the peak. We can see clearly that the moving peakon profile is resolved very well. There is no numerical oscillation observed. The results for the both schemes match the exact solution very well.

Example 3.3. Two-peakon interaction

In this example we consider the two-peakon interaction [18, 24] of the DP equation (3.1) with the initial condition

$$u_0(x)=\phi_1(x)+\phi_2(x), \tag{3.4}$$

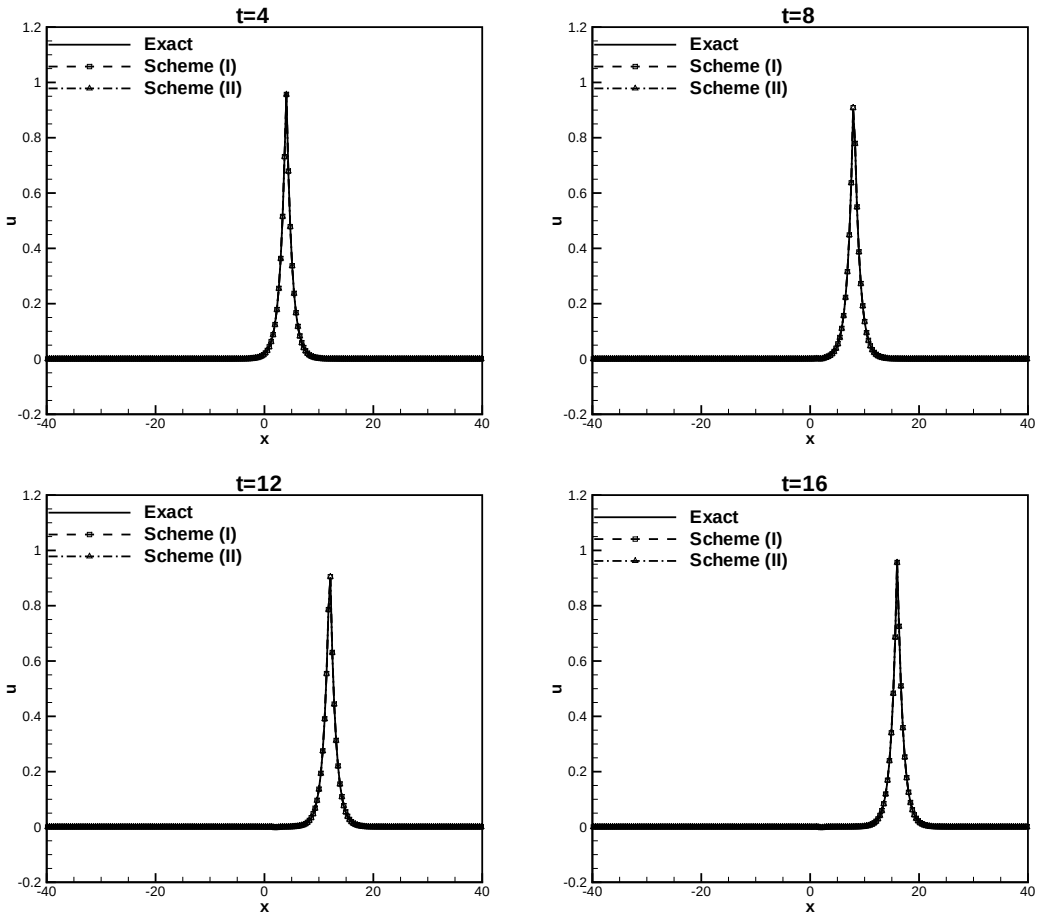

Figure 2: The peakon profile of the DP equation (3.1) with the exact solution (3.2). Periodic boundary condition in $[-40,40]$. P^4 elements and a uniform mesh with $N=228$ cells.

where

$$\phi_i(x)=c_i e^{-|x-x_i|}, \quad i=1,2. \tag{3.5}$$

We also consider the two-anti-peakon interaction of the DP equation with the initial condition

$$u_0(x)=\psi_1(x)+\psi_2(x), \tag{3.6}$$

where

$$\psi_i(x)=-c_i e^{-|x+x_i|}, \quad i=1,2. \tag{3.7}$$

The parameters are $c_1=2$, $c_2=1$, $x_1=-13.792$, $x_2=-4$. The computational domain is $[-40,40]$. We use the P^3 element with $N=512$ cells in our computation of the LDG

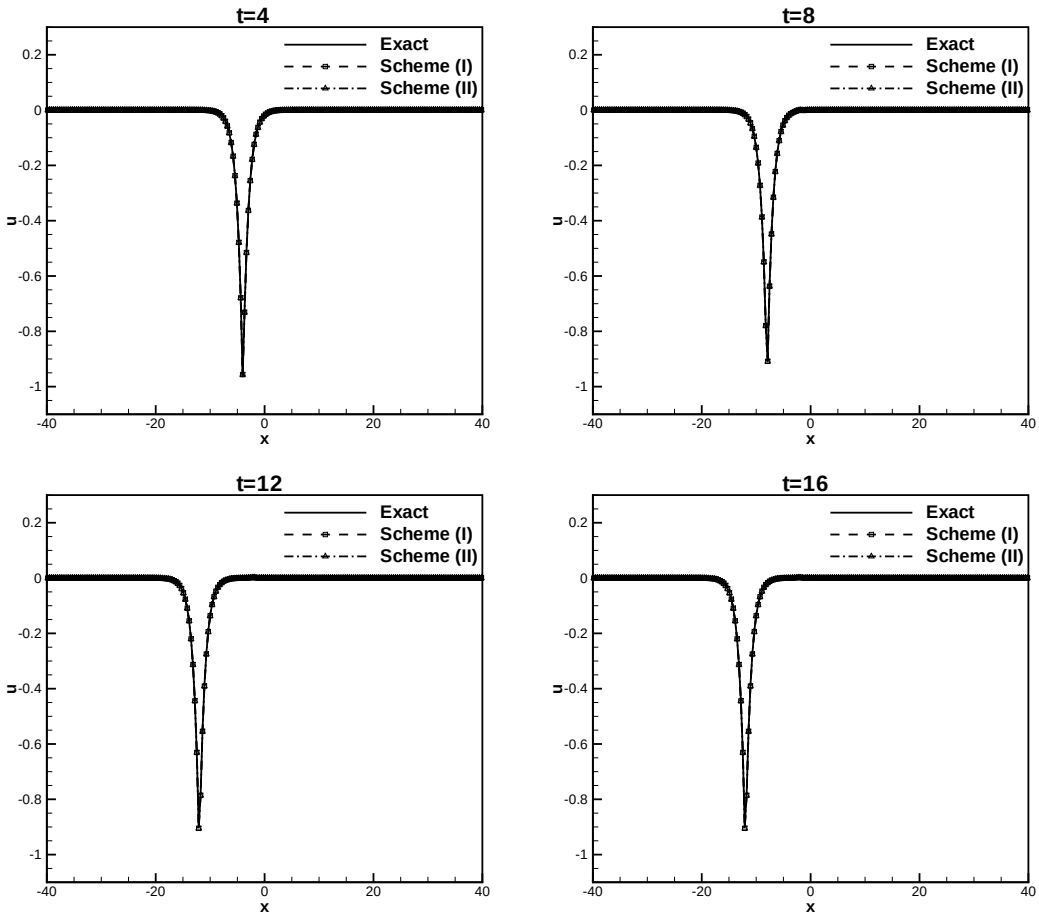

Figure 3: The anti-peakon profile of the DP equation (3.1) with the exact solution (3.3). Periodic boundary condition in $[-40,40]$. P^4 elements and a uniform mesh with $N=228$ cells.

method. In Figs. 4 and 5, the interaction at $t=0$, 4, 8, 10, 12 and 16 are shown. It is very easy to occur numerical oscillation during the interaction of the two-peakon or two-anti-peakon. We can see clearly that the moving peakon interaction by the both methods is resolved very well.

Example 3.4. Shock peakon solution

In this example, we present the wave evolution of the shock peakon solution

$$u(x,t)=-\frac{1}{1+t}\text{sign}(x)e^{-|x|}. \tag{3.8}$$

The computational domain is $[-30,30]$. In Fig. 6, the shock peakon profile at $t=0$, 1, 2 and 6 are shown. The lack of smoothness of shock peakon introduces high-frequency errors into the calculation and will cause the numerical oscillation near the shock peakon. To

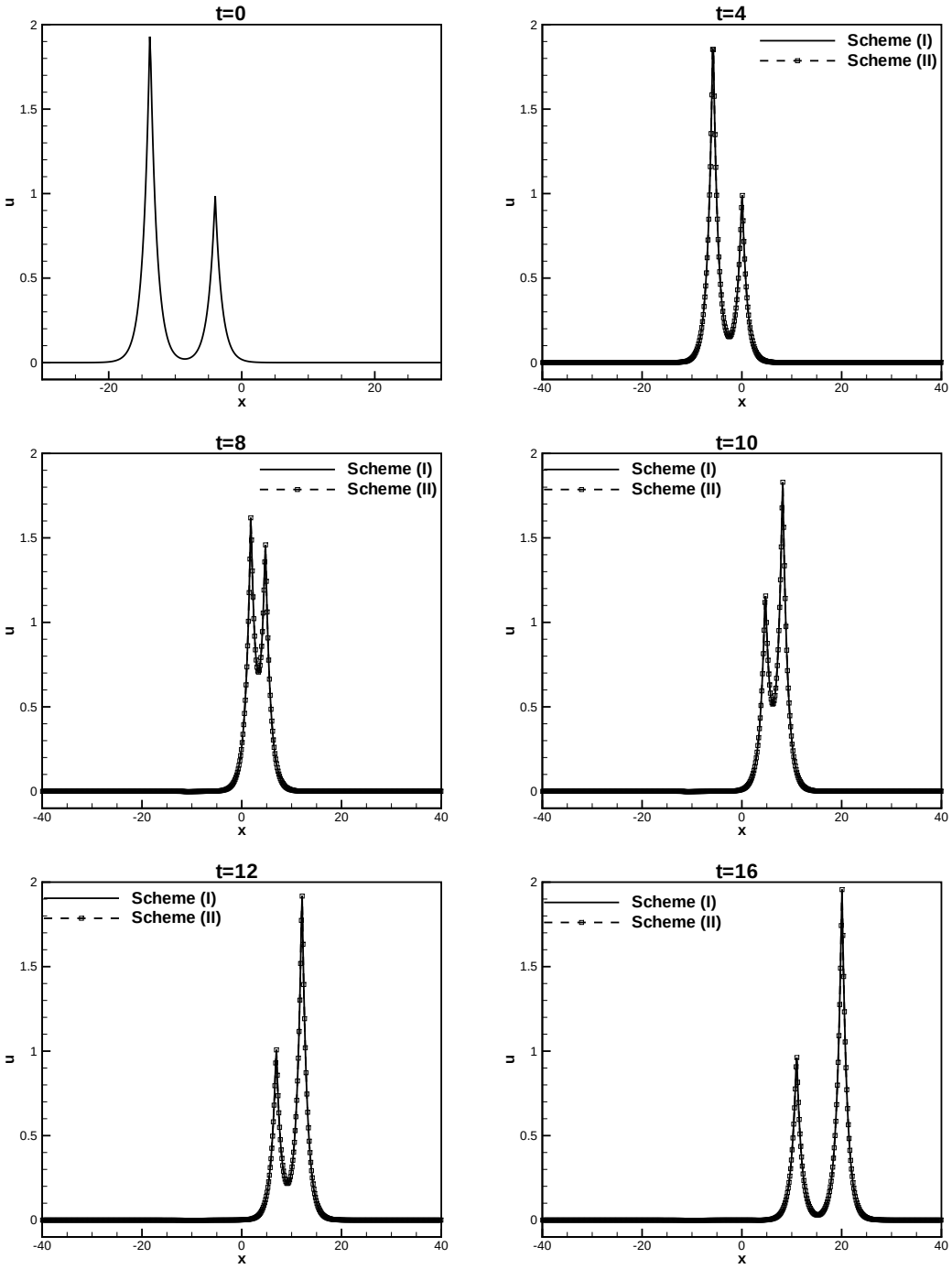

Figure 4: The two-peakon interaction of the DP equation (3.1) with the initial condition (3.4). Periodic boundary condition in $[-40,40]$. P^3 elements and a uniform mesh with $N=512$ cells.

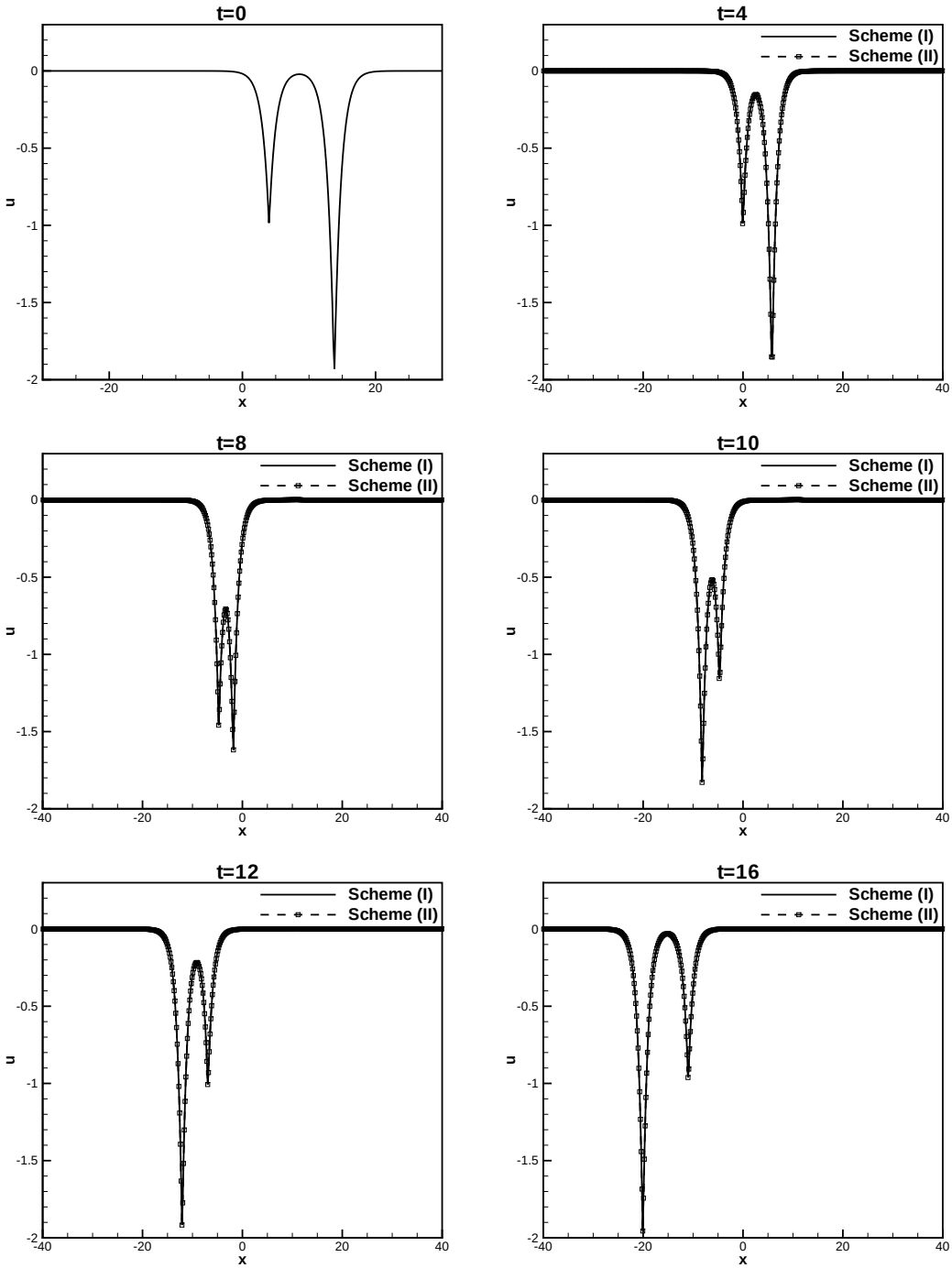

Figure 5: The two-anti-peakon interaction of the DP equation (3.1) with the initial condition (3.6). Periodic boundary condition in $[-40,40]$. P^3 elements and a uniform mesh with $N=512$ cells.

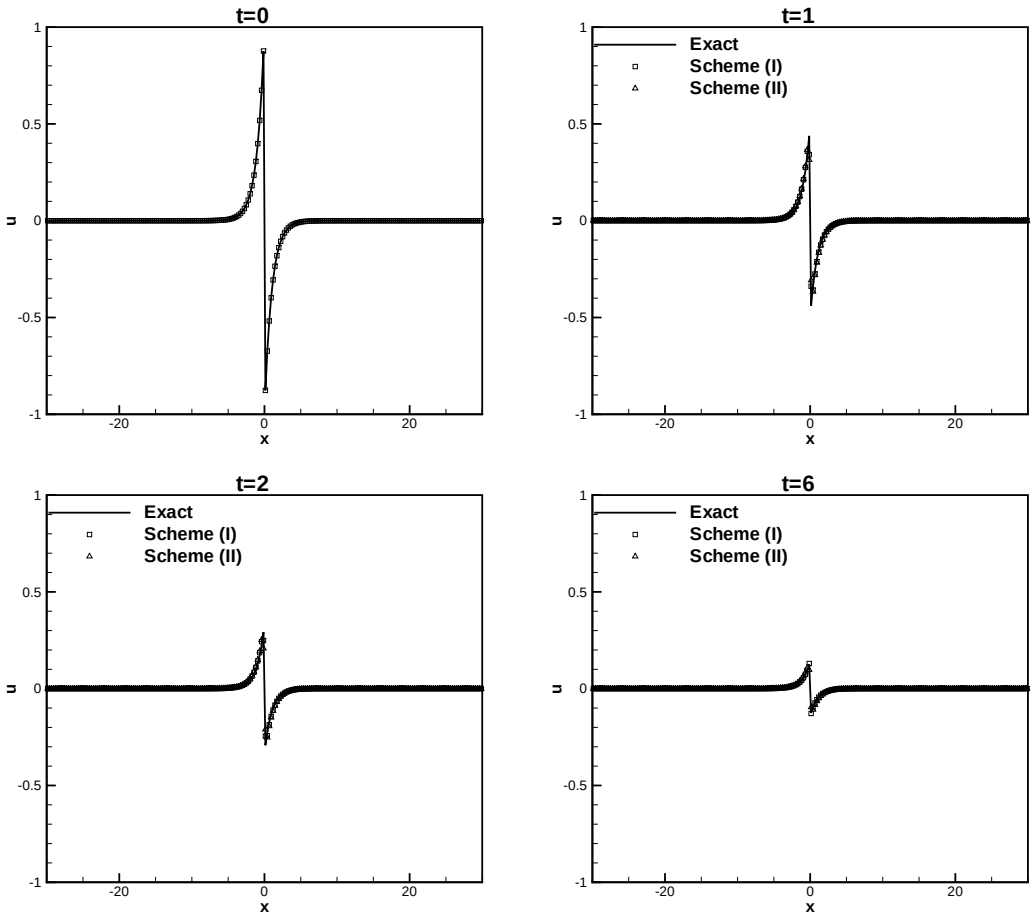

Figure 6: Shock peakon solution of the DP equation (3.1) with the exact solution (3.3). Periodic boundary condition in $[-30,30]$. P^4 elements and a uniform mesh with $N=228$ cells.

control the oscillation of u_h, we use the TVBM limiter in [4] to remove the oscillation near the discontinuity of u_h. In our computation of the LDG method, we use the P^4 element with $N=228$ cells to resolve the shock peakon. We can see clearly that the shock peakon profile is resolved very well. The shock interface is very sharp and there is no numerical oscillation observed for the both schemes.

Example 3.5. Shock formation

In this example we consider the shock formation [11,18] of the DP equation (3.1) with the initial condition

$$u_0(x)=e^{0.5x^2}\sin(\pi x). \tag{3.9}$$

The computational domain is $[-2,2]$. We use the P^3 element with $N=256$ cells in our computation of the LDG method. In Fig. 7, the shock peakon profile at $t=0$, 0.12, 0.18,

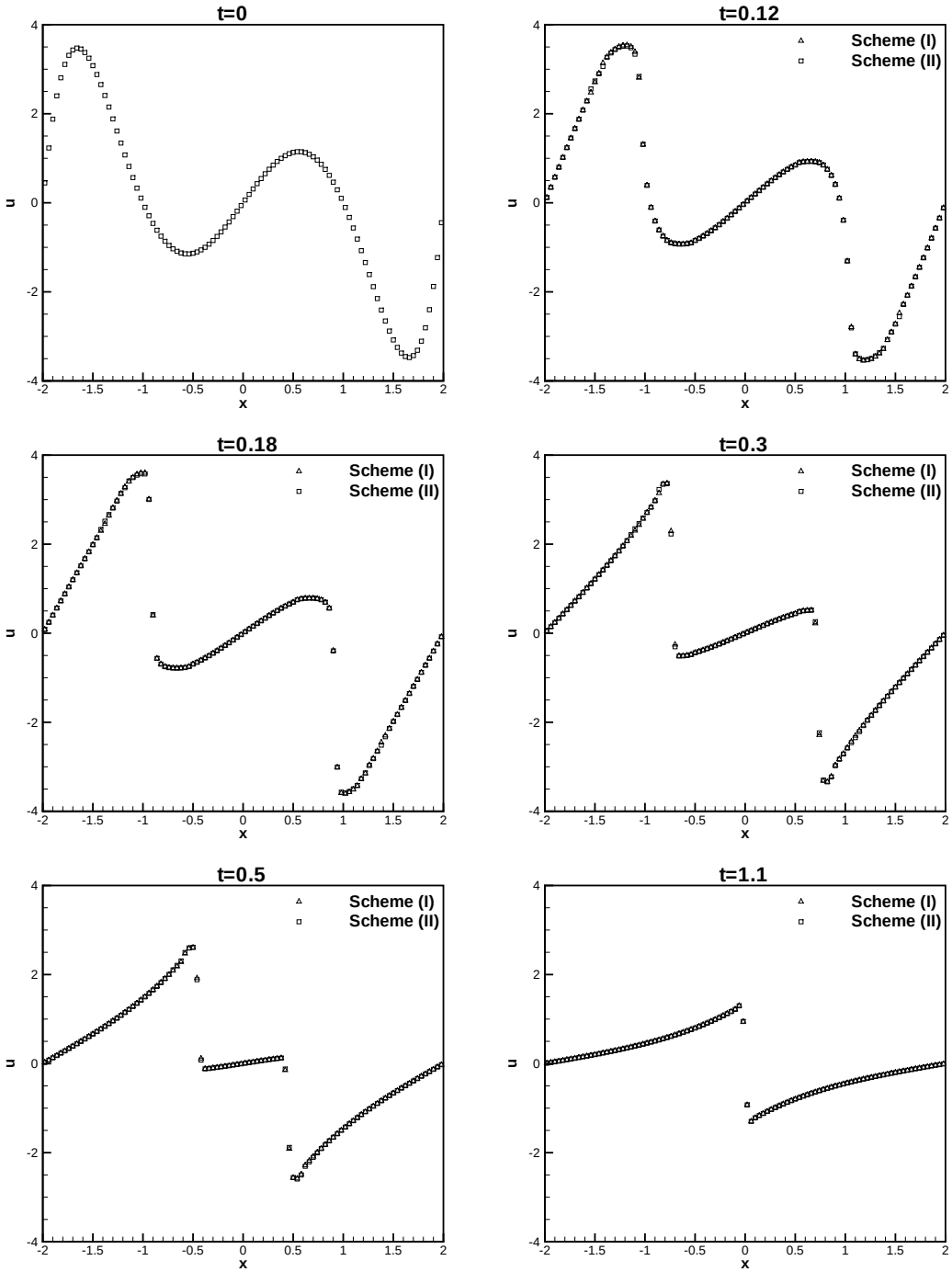

Figure 7: Shock formation of the DP equation (3.1) with the initial condition (3.9). Periodic boundary condition in $[-2,2]$. P^3 elements and a uniform mesh with $N=100$ cells.

0.3, 0.5 and 1.1 are shown. To control the oscillation of u_h, we use the TVBM limiter in [4] to remove the oscillation near the discontinuity of u_h when the shock is formed. The shock interface is very sharp. There are only two transition points in the position of shock and no numerical oscillation observed. The results agree with those in [11, 18].

Example 3.6. Peakon and anti-peakon interaction

In this example we consider the peakon and interaction [18, 24] of the DP equation (3.1) with the initial condition

$$u_0(x) = c_1 e^{-|x-x_1|} - c_2 e^{-|x-x_2|}. \tag{3.10}$$

Firstly, we consider the symmetric case and choose the parameters $c_1 = 1$, $c_2 = 1$, $x_1 = -5$, $x_2 = 5$. In Fig. 8, the interaction at $t = 0$, 2, 4, 5, 6 and 7 are shown. We can see that a stationary shock peakon is formed at $t \approx 5$ and evolution follows one shock peakon solution.

Secondly, we consider the nonsymmetric case and choose the parameters $c_1 = 2$, $c_2 = 1$, $x_1 = -5$, $x_2 = 5$. In Fig. 9, the interaction at $t = 0$, 2, 3, 3.3626, 4 and 6 are shown. We can see that a stationary shock peakon is formed at $t \approx 3.3626$ and evolution follows one shock peakon solution.

The computational domain is $[-25,25]$. We use the P^3 element with $N = 256$ cells in our computation of the LDG method. To control the oscillation of u_h, we use the TVBM limiter in [4] to remove the oscillation near the discontinuity of u_h when the shock peakon is formed. In both cases, we can see clearly from Fig. 10 that the interaction is resolved very well. Both schemes can automatically capture the shock and shock interface is very sharp. Only on or two transition points are observed and there is no numerical oscillation during the peakon and anti-peakon interaction.

Example 3.7. Triple interaction

In this example we consider the peakon, shock peakon and anti-peakon interaction [11, 18] of the DP equation (3.1) with the initial condition

$$u_0(x) = e^{-|x-5|} + \text{sign}(x) e^{-|x|} - e^{-|x-5|}. \tag{3.11}$$

The computational domain is $[-25,25]$. We use the P^3 element with $N = 256$ cells in our computation of the LDG method. To control the oscillation of u_h, we use the TVBM limiter in [4] to remove the oscillation near the discontinuity of u_h when the shock peakon is formed. We can see clearly that the interaction is resolved very well. The shock interfaces are very sharp. There is only one transition point observed in each shock.

4 Concluding remarks

We have developed two local discontinuous Galerkin methods to solve the DP equation. L^2 stability is proven for general solutions. TVB property of the DG scheme for the P^0

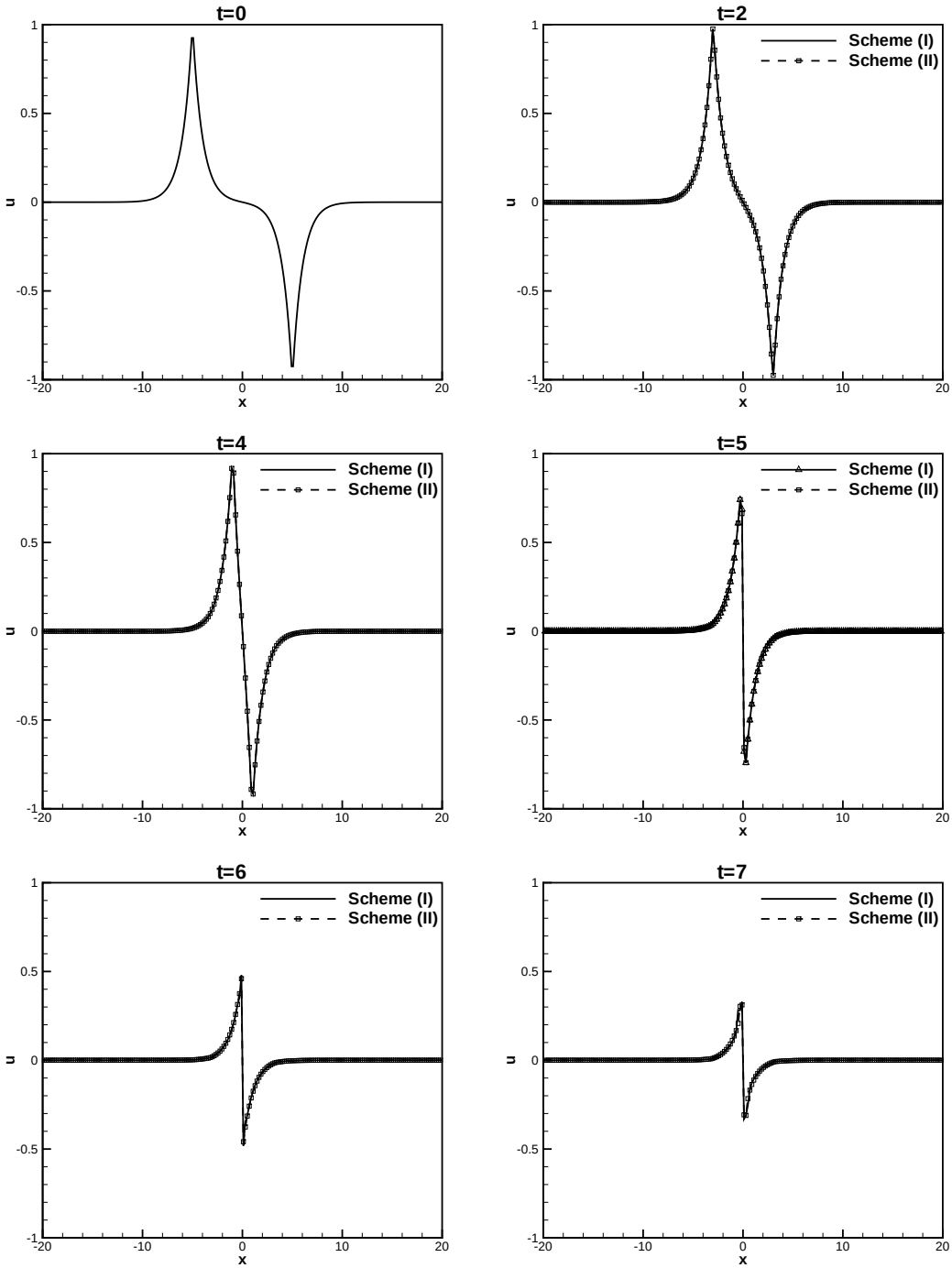

Figure 8: Symmetric peak and antipeak interaction of the DP equation (3.1). Periodic boundary condition in $[-25,25]$. P^3 elements and a uniform mesh with $N=256$ cells.

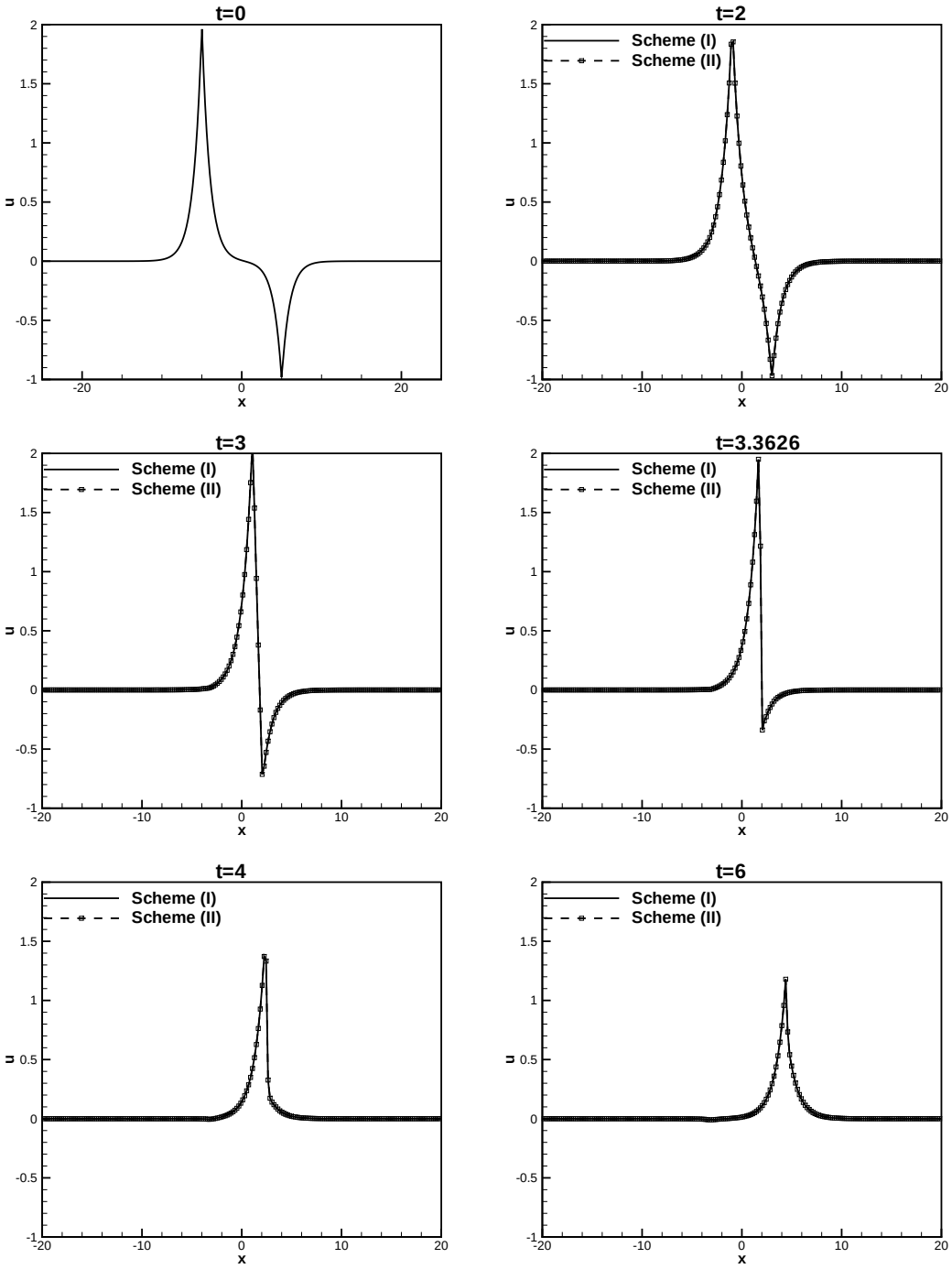

Figure 9: Nonsymmetric peak and antipeak interaction of the DP equation (3.1). Periodic boundary condition in $[-25,25]$. P^3 elements and a uniform mesh with $N=256$ cells.

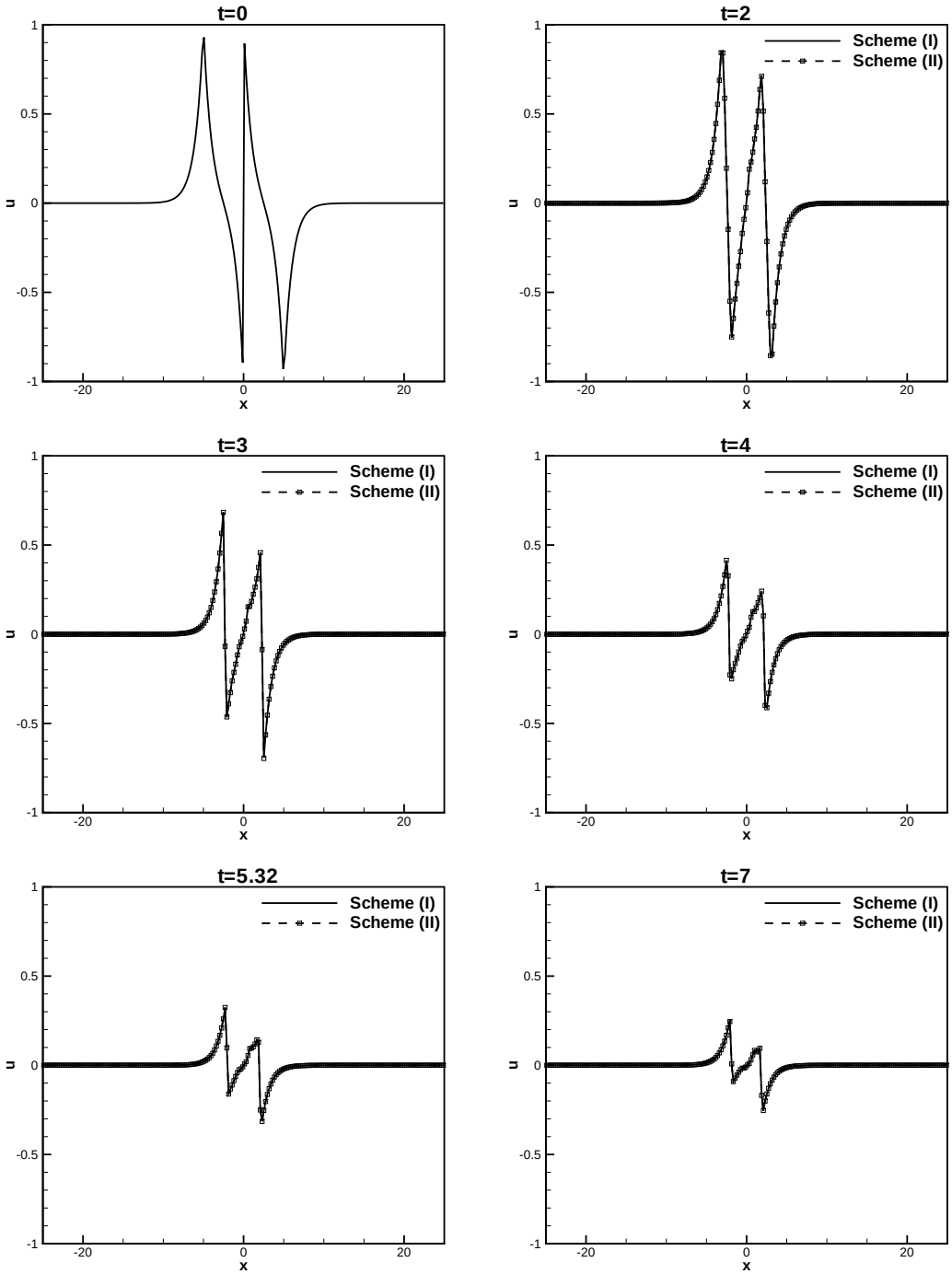

Figure 10: Peakon, shock peakon and anti-peakon interaction of the DP equation (3.1) with the initial condition (3.11). Periodic boundary condition in $[-25,25]$. P^3 elements and a uniform mesh with $N=256$ cells.

case is proved. Numerical examples are given to illustrate the accuracy and capability of the methods.

An important issue not addressed in this paper is the a priori error estimates of solutions. From the stability and approximation results, we can derive L^2 a priori error estimates of the high order LDG method for the Camassa-Holm equation [34]. However the proof of the high order LDG method for the DP equation is not straightforward and we could easily lose half an order or even one order in accuracy, because of a lack of control for certain jump terms at cell boundaries. Such error estimates are left for future work.

Acknowledgments

The research of the first author is supported by NSFC grant 10971211, FANEDD, FANEDD of CAS and the Fundamental Research Funds for the Central Universities. Additional support is provided by the Alexander von Humboldt-Foundation while the author was in residence at Freiburg University, Germany. The research of the second author is supported by ARO grant W911NF-08-1-0520 and NSF grant DMS-0809086.

Appendix: Proof of Lemma 2.2

We will give the proof of Lemma 2.2 in this appendix. First, we rewrite the matrix $\mathbf{A}$ into the following form

$$\mathbf{A}=a\mathbf{B}, \qquad a=\frac{1}{h^2}, \tag{A.1}$$

where the matrix $\mathbf{B}$ is

$$\mathbf{B}=\begin{pmatrix} b & -1 & 0 & \cdots & 0 & -1 \\ -1 & b & -1 & 0 & \cdots & 0 \\ 0 & -1 & b & -1 & 0 & 0 \\ \vdots & \vdots & \ddots & \ddots & \ddots & \vdots \\ 0 & \cdots & 0 & -1 & b & -1 \\ -1 & 0 & \cdots & 0 & -1 & b \end{pmatrix}, \qquad b=\frac{1+2a}{a}=h^2+2. \tag{A.2}$$

Then the inverse of the matrix $\mathbf{A}$ becomes

$$\mathbf{A}^{-1}=\frac{1}{a}\mathbf{B}^{-1}=h^2\mathbf{B}^{-1}. \tag{A.3}$$

In the following we will only discuss the properties of the matrix $\mathbf{B}$.

Lemma A.1. *(*Explicit form of the matrix $\mathbf{B}^{-1}$*) The inverse of the matrix* $\mathbf{B}$ *can be written as*

$$\mathbf{B}^{-1}=\begin{pmatrix} \beta_1 & \beta_2 & \cdots & \beta_{J-1} & \beta_J \\ \beta_J & \beta_1 & \beta_2 & \cdots & \beta_{J-1} \\ \vdots & \vdots & \ddots & \cdots & \vdots \\ \beta_3 & \cdots & \beta_J & \beta_1 & \beta_2 \\ \beta_2 & \cdots & \beta_{J-1} & \beta_J & \beta_1 \end{pmatrix}. \tag{A.4}$$

Proof. From the results in [15], we can get the explicit form the matrix $\mathbf{B^{-1}}$ as the following

$$(\mathbf{B}^{-1})_{i,j}=\theta_{i,j}=\frac{1}{\gamma_{J+1}-\gamma_{J-1}-2}\big(\gamma_{J-j+1}\gamma_i-\gamma_{J-j}\gamma_{i-1}+\gamma_{j-i}\big), \tag{A.5}$$

where

$$\gamma_k=\frac{\mu_1^k-\mu_2^k}{\mu_1-\mu_2},\qquad \mu_1=\frac{1}{2}(b+\sqrt{b^2-4}),\qquad \mu_2=\frac{1}{2}(b-\sqrt{b^2-4}). \tag{A.6}$$

Here we notice that $\mu_1\mu_2=1$, $\mu_1>1$ and $\mu_2<1$. Using the definition of γ_k and some algebra calculation, we can prove that

$$\theta_{i,j}=\theta_{i+1,j+1}. \tag{A.7}$$

Due to the symmetry of the matrix $\mathbf{B}$, we know that $\theta_{i,j}=\theta_{j,i}$. We denote

$$\beta_j=\theta_{1,j}=\frac{1}{\gamma_{J+1}-\gamma_{J-1}-2}\big(\gamma_{J-j+1}+\gamma_{j-1}\big),\qquad \beta_j=\beta_{J-j+2}. \tag{A.8}$$

Now we can easily see that the matrix $\mathbf{B}^{-1}$ has the form (A.4). □

Lemma A.2. $\{\beta_j\}$ *in Lemma A.*1 *satisfy the following properties*

$$|\beta_j-\beta_{j+1}|<\frac{1}{2},\quad j=1,\cdots,J-1, \tag{A.9}$$

$$0\leqslant\beta_1-\beta_J<\frac{1}{2}. \tag{A.10}$$

Proof. From the definition of γ_k, we can have

$$\begin{aligned}\gamma_{k+1}-\gamma_k-1&=\frac{1}{\mu_1-\mu_2}(\mu_1^{k+1}-\mu_2^{k+1}-\mu_1^k+\mu_2^k-\mu_1+\mu_2)\\&=\frac{1}{\mu_1-\mu_2}\big((\mu_1-1)(\mu_1^k-1)-(\mu_2^k-1)(\mu_2-1)\big).\end{aligned}$$

Using the property of $\mu_1\mu_2=1$, we can obtain

$$\gamma_{k+1}-\gamma_k-1=\frac{\mu_1-1}{\mu_1-\mu_2}(\mu_1^k-1)(1-\mu_2^{k+1}). \tag{A.11}$$

Similarly, we can also get the following equality

$$\gamma_j-\gamma_{j-1}-1=\frac{\mu_1-1}{\mu_1-\mu_2}(\mu_1^{j-1}-1)(1-\mu_2^j), \tag{A.12}$$

$$\gamma_{J-j+1}-\gamma_{J-j}-1=\frac{\mu_1-1}{\mu_1-\mu_2}(\mu_1^{J-j}-1)(1-\mu_2^{J-j+1}), \tag{A.13}$$

$$\gamma_J-\gamma_{J-1}-1=\frac{\mu_1-1}{\mu_1-\mu_2}(\mu_1^{J-1}-1)(1-\mu_2^J), \tag{A.14}$$

$$\gamma_{J+1}-\gamma_{J-1}-2=\frac{\mu_1-1}{\mu_1-\mu_2}(\mu_1^J-1)(1+\mu_2)(1-\mu_2^J). \tag{A.15}$$

Now we will estimate the difference of $\{\beta_j\}$.

$$\begin{aligned}\beta_j-\beta_{j+1}&=\frac{1}{\gamma_{J+1}-\gamma_{J-1}-2}(\gamma_{J-j+1}-\gamma_{j-1}-(\gamma_{J-j}-\gamma_j))\\&=\frac{1}{\gamma_{J+1}-\gamma_{J-1}-2}(\gamma_{J-j+1}-\gamma_{J-j}-1-(\gamma_j-\gamma_{j-1}-1))\\&=\frac{(\mu_1^{J-j}-1)(1-\mu_2^{J-j+1})-(\mu_1^{j-1}-1)(1-\mu_2^j)}{(\mu_1^J-1)(1+\mu_2)(1-\mu_2^J)}.\end{aligned}$$

Using the property of $\mu_1\mu_2=1$ again and after some algebra calculation, we obtain

$$\beta_j-\beta_{j+1}=\frac{\mu_1^{J-j+1}-\mu_1^j}{(\mu_1^J-1)(1+\mu_1)}. \tag{A.16}$$

Due to $\mu_1>1$, we can get

$$\begin{aligned}&\mu_1^{J-j+1}-\mu_1^j\leqslant\mu_1^J-1\implies\beta_j-\beta_{j+1}\leqslant\frac{1}{1+\mu_1}<\frac{1}{2},\\&\mu_1^{J-j+1}-\mu_1^j\geqslant 1-\mu_1^J\implies\beta_j-\beta_{j+1}\geqslant-\frac{1}{1+\mu_1}>-\frac{1}{2}.\end{aligned}$$

Then we have proved (A.9). For (A.10), we have

$$\beta_1-\beta_J=\frac{\gamma_J-\gamma_{J-1}-1}{\gamma_{J+1}-\gamma_{J-1}-2}=\frac{\mu_1^{J-1}-1}{(\mu_1^J-1)(1+\mu_2)}=\frac{\mu_1^J-\mu_1}{\mu_1^{J+1}-1+\mu_1^J-\mu_1}.$$

Due to $\mu_1>1$, we know $\beta_1-\beta_J\geqslant 0$. We also have

$$\mu_1^{J+1}-1>0,\quad \mu_1^J-\mu_1\geqslant 0,\quad \mu_1^{J+1}-1-(\mu_1^J-\mu_1)=(1+\mu^J)(\mu_1-1)>0,$$

i.e.,

$$\mu_1^{J+1}-1>\mu_1^J-\mu_1.$$

Then we have

$$\beta_1-\beta_J<\frac{\mu_1^J-\mu_1}{2(\mu_1^J-\mu_1)}=\frac{1}{2}.$$

The proof of the lemma is thus finished. □

From the results of Lemmas A.1 and A.2, we can directly get the results in Lemma 2.2.

References

[1] F. Bassi, and S. Rebay, A high-order accurate discontinuous finite element method for the numerical solution of the compressible Navier-Stokes equations, J. Comput. Phys., 131 (1997), 267–279.
[2] B. Cockburn, S. Hou, and C.-W. Shu, The Runge-Kutta local projection discontinuous Galerkin finite element method for conservation laws IV: the multidimensional case, Math. Comput., 54 (1990), 545–581.
[3] B. Cockburn, S.-Y. Lin, and C.-W. Shu, TVB Runge-Kutta local projection discontinuous Galerkin finite element method for conservation laws III: one dimensional systems, J. Comput. Phys., 84 (1989), 90–113.
[4] B. Cockburn, and C.-W. Shu, TVB Runge-Kutta local projection discontinuous Galerkin finite element method for conservation laws II: general framework, Math. Comput., 52 (1989), 411–435.
[5] B. Cockburn, and C.-W. Shu, The local discontinuous Galerkin method for time-dependent convection-diffusion systems, SIAM J. Numer. Anal., 35 (1998), 2440–2463.
[6] B. Cockburn, and C.-W. Shu, The Runge-Kutta discontinuous Galerkin method for conservation laws V: multidimensional systems, J. Comput. Phys., 141 (1998), 199–224.
[7] B. Cockburn, and C.-W. Shu, Foreword for the special issue on discontinuous Galerkin method, J. Sci. Comput., 22-23 (2005), 1–3.
[8] B. Cockburn, and C.-W. Shu, Foreword for the special issue on discontinuous Galerkin method, J. Sci. Comput., 40 (2009), 1–3.
[9] G. Coclite, and K. Karlsen, On the well-posedness of the Degasperis-Procesi equation, J. Funct. Anal., 233 (2006), 60–91.
[10] G. Coclite, and K. Karlsen, On the uniqueness of discontinuous solutions to the Degasperis-Procesi equation, J. Differential Equations, 234 (2007), 142–160.
[11] G. Coclite, K. Karlsen, and N. Risebro, Numerical schemes for computing discontinuous solutions of the Degasperis-Procesi equation, IMA J. Numer. Anal., 28 (2008), 8–105.
[12] C. Dawson, Foreword for the special issue on discontinuous Galerkin method, Comput. Meth. Appl. Mech. Eng., 195 (2006), 3183.
[13] A. Degasperis, D. Holm, and A. Hone, A new integrable equation with peakon solutions, Theoret. Math. Phys., 133 (2002), 1463–1474.

[14] A. Degasperis, and M. Procesi, Asymptotic integrability, in A. Degasperis and G. Gaeta, editors, Symmetry and Perturbation Theory, 23–37, World Sci. Publ., River Edge, NJ, 1999.
[15] M. El-Shehawey, G. El-Shreef, and A. Al-Henawy, Analytical inversion of general periodic tridiagonal matrices, J. Math. Anal. Appl., 345 (2008), 123–134.
[16] J. Escher, Y. Liu, and Z. Yin, Global weak solutions and blow-up structure for the Degasperis-Procesi equation, J. Funct. Anal., 241 (2006), 457–485.
[17] J. Escher, Y. Liu, and Z. Yin, Shock waves and blow-up phenomena for the periodic Degasperis-Procesi equation, Indiana Univ. Math. J., 56 (2007), 87–117.
[18] B. Feng, and Y. Liu, An operator splitting method for the Degasperis-Procesi equation, J. Comput. Phys., 228 (2009), 7805–7820.
[19] J. Hesthaven, and T. Warburton, Nodal Discontinuous Galerkin Methods, Algorithms, Analysis, and Applications, Springer, 2008.
[20] H. Hoel, A numerical scheme using multi-shockpeakons to compute solutions of the Degasperis-Procesi equation, Electron. J. Differential Equations, 2007 (2007), 1–22.
[21] J. Lenells, Traveling wave solutions of the Degasperis-Procesi equation, J. Math. Anal. Appl., 306 (2005), 72–82.
[22] B. Li, Discontinuous Finite Elements in Fluid Dynamics and Heat Transfer, Springer-Verlag, London, 2006.
[23] Y. Liu, and Z. Yin, Global existence and blow-up phenomena for the Degasperis-Procesi equation, Commun. Math. Phys., 267 (2006), 801–820.
[24] H. Lundmark, Formation and dynamics of shock waves in the Degasperis-Procesi equation, J. Nonlinear. Sci., 17 (2007), 169–198.
[25] H. Lundmark, and J. Szmigielski, Multi-peakon solutions of the Degasperis-Procesi equation, Inverse. Prob., 19 (2003), 1241–1245.
[26] H. Lundmark, and J. Szmigielski, Degasperis-Procesi peakons and the discrete cubic string, IMRP Int. Math. Res. Pap., 2 (2005), 53–116.
[27] Y. Matsuno, Multisoliton solutions of the Degasperis-Procesi equation and their peakon limit, Inverse. Prob., 21 (2005), 1553–1570.
[28] Y. Matsuno, The N-soliton solution of the Degasperis-Procesi equation, Inverse. Prob., 21 (2005), 2085–2101.
[29] W. Reed, and T. Hill, Triangular Mesh Methods for the Neutrontransport Equation, La-ur-73-479, Los Alamos Scientific Laboratory, 1973.
[30] B. Riviére, Discontinuous Galerkin Methods for Solving Elliptic and Parabolic Equations, Theory and Implementation, SIAM, 2008.
[31] C.-W. Shu, Discontinuous Galerkin methods: general approach and stability, in S. Bertoluzza, S. Falletta, G. Russo, and C.-W. Shu, editors, Numerical Solutions of Partial Differential Equations, 149–201, Birkhauser, Basel, 2009.
[32] C.-W. Shu, and S. Osher, Efficient implementation of essentially non-oscillatory shock-capturing schemes, J. Comput. Phys., 77 (1988), 439–471.
[33] Y. Xu, and C.-W. Shu, Local discontinuous Galerkin methods for two classes of two dimensional nonlinear wave equations, Phys. D., 208 (2005), 21–58.
[34] Y. Xu, and C.-W. Shu, A local discontinuous Galerkin method for the Camassa-Holm equation, SIAM J. Numer. Anal., 46 (2008), 1998–2021.
[35] Y. Xu, and C.-W. Shu, Local discontinuous Galerkin method for the Hunter-Saxton equation and its zero-viscosity and zero-dispersion limit, SIAM J. Sci. Comput., 31 (2008), 1249–1268.
[36] Y. Xu, and C.-W. Shu, Local discontinuous Galerkin methods for high-order time-dependent partial differential equations, Commun. Comput. Phys., 7 (2010), 1–46.

[37] Y. Xu, and C.-W. Shu, Dissipative numerical methods for the Hunter-Saxton equation, J. Comput. Math., 28 (2010), 606–620.
[38] J. Yan, and C.-W. Shu, A local discontinuous Galerkin method for KdV type equations, SIAM J. Numer. Anal., 40 (2002), 769–791.
[39] Z. Yin, Global existence for a new periodic integrable equation, J. Math. Anal. Appl., 283 (2003), 129–139.
[40] Z. Yin, On the Cauchy problem for an integrable equation with peakon solutions, Illinois J. Math., 47 (2003), 649–666.
[41] Z. Yin, Global weak solutions for a new periodic integrable equation with peakon solutions, J. Funct. Anal., 212 (2004), 182–194.